**Biological insights in the pathogenesis of hypermobile Ehlers-Danlos syndrome from proteome profiling of patients' dermal myofibroblasts**

Nicola Chiarelli[1#], Nicoletta Zoppi[1#], Marco Ritelli[1], Marina Venturini[2], Daniele Capitanio[3], Cecilia Gelfi[3,4], Marina Colombi[1*]

**Affiliations**

[1]Division of Biology and Genetics, Department of Molecular and Translational Medicine, University of Brescia, Brescia, Italy

[2]Division of Dermatology, Department of Clinical and Experimental Sciences, Spedali Civili University Hospital Brescia, Italy

[3] Department of Biomedical Sciences for Health, University of Milan, Milano, Italy

[4] IRCCS Istituto ortopedico Galeazzi, Milan, Italy

[#] These authors contributed equally to this work

***Corresponding author**

Prof. Marina Colombi
Division of Biology and Genetics
Department of Molecular and Translational Medicine
University of Brescia
Viale Europa 11
25123 Brescia, Italy
Phone/Fax +39 030 3717240
e-mail: marina.colombi@unibs.it

**Abstract**

Hypermobile Ehlers-Danlos syndrome (hEDS), mainly characterized by generalized joint hypermobility and its complications, minor skin changes, and apparently segregating with an autosomal dominant pattern, is still without a known molecular basis. Hence, its diagnosis is only clinical based on a strict set of criteria defined in the revised EDS nosology. Moreover, the hEDS phenotypic spectrum is wide-ranging and comprises multiple associated signs and symptoms shared with other heritable or acquired connective tissue disorders and chronic inflammatory diseases. In this complex scenario, we previously demonstrated that patients' skin fibroblasts show phenotypic features of myofibroblasts, widespread extracellular matrix (ECM) disarray, perturbation of ECM-cell contacts, and dysregulated expression of genes involved in connective tissue architecture and related to inflammatory and pain responses. Herein, the cellular proteome of 6 hEDS dermal myofibroblasts was compared to that of 12 control fibroblasts to deepen the knowledge on mechanisms involved in the disease pathogenesis. Qualitative and quantitative differences were assessed based on top-down and bottom-up approaches and some differentially expressed proteins were proofed by biochemical analyses. Proteomics disclosed the differential expression of proteins principally implicated in cytoskeleton organization, energy metabolism and redox balance, proteostasis, and intracellular trafficking. Our findings offer a comprehensive view of dysregulated protein networks and related pathways likely associated with the hEDS pathophysiology. The present results can be regarded as a starting point for future in-depth investigations aimed to decipher the functional impact of potential bioactive molecules for the development of targeted management and therapies.

**Keywords**: Hypermobile Ehlers-Danlos syndrome; myofibroblasts; proteome profiling; cytoskeleton remodeling and signalling; metabolic changes; S100A4.

**Abbreviations**: Annexin A2 (ANXA2), α-parvin (PARVA), α-smooth muscle actin (α-SMA), β-actin (ACTB), cofilin-1 (CFL1), cofilin-2 (CFL2), conditioned medium (CM), damage-associated molecular patterns (DAMPs), differentially expressed proteins (DEPs), endoplasmic reticulum (ER), extracellular matrix (ECM), false discovery rate (FDR), fibroblast-to-myofibroblast transition (FMT), fibronectin (FN), filamin A (FLNA), filamin C (FLNC), gene ontology (GO), glyceraldehyde-3-phosphate dehydrogenase (GAPDH), hypermobile Ehlers-Danlos syndrome (hEDS), heritable connective tissue disorder (HCTD), immunofluorescence microscopy (IF), integrin linked kinase (ILK), liquid chromatography with tandem mass spectrometry (LC-MS/MS), lactate dehydrogenase B (LDHB), matrix metalloproteinases (MMPs), matrix-assisted laser desorption/ionization mass spectrometry (MALDI-TOF MS), minimum information about a proteomics experiment-gel electrophoresis (MIAPE-GE), monoclonal antibody (mAb), myosin IC (MYO1C), non-muscle actin β (β-actin), peptide mass fingerprint (PMF), pyruvate kinase M1/2 (PKM), protein disulfide isomerase family A member 3 (PDIA3), RAB1B, member RAS oncogene family (Rab1b), Rac family small GTPase 1 (RAC1), reactive oxidative species (ROS), S100 calcium binding protein A4 (S100A4), two-dimensional difference in-gel electrophoresis (2D-DIGE), vimentin (VIM), western blotting (WB).

## Highlights

- Hypermobile Ehlers Danlos syndrome (hEDS) is orphan of a genetic etiology
- *In vitro* cultured hEDS dermal fibroblasts show a myofibroblast-like phenotype
- Proteome profiling of hEDS myofibroblasts to add insights into disease mechanisms
- hEDS cell differentiation may involve cytoskeleton signaling and metabolic changes
- S100A4 as potential key disease molecule and therapeutic target in hEDS

## 1. Introduction

Hypermobile Ehlers-Danlos syndrome (hEDS) is a multisystemic heritable connective tissue disorder (HCTD) that significantly decreases patients' quality of life [1–3]. Despite hEDS is likely the most common HCTD and in the last years several efforts have been made in attempting to disclose (a) causal gene(s), it remains without a known molecular basis. hEDS is considered an autosomal dominant condition with nearly complete penetrance, variable expressivity within and between families, marked age- and sex-dependent variability, and is diagnosed only clinically, since no instrumental, histopathological/ultrastructural, and molecular findings are yet considered beyond-any-doubt diagnostic. The current EDS nosology defined a set of strict criteria for hEDS that is determined by the presence of generalized joint hypermobility; two or more items among systemic involvement, positive family history and musculoskeletal involvement; and the exclusion of other hereditary and acquired CTDs [2].

The hEDS phenotypic spectrum is wide-ranging and comprises a range of comorbidities not included in the up-to-date nosology, such as functional gastrointestinal dysfunctions (e.g. gastrointestinal pain, gastroesophageal reflux disease, gastrointestinal dysmotility, irritable bowel disease), pelvic and bladder dysfunctions, mast cell activation syndrome, orthostatic intolerance, postural orthostatic tachycardia syndrome, and a range of psychological issues associated with pain such as depression, anxiety, sleep disturbance, headache, and migraine, although the underlying causes remain to be explored [1,3].

In this confusing scenario, our earlier works provided some evidence to unveil the disease mechanisms likely contributing to the hEDS pathogenesis [4,5]. Indeed, we demonstrated that hEDS dermal fibroblasts compared to control cells show the differential expression of genes mainly involved in extracellular matrix (ECM) organization, cell-cell and cell-ECM interactions, and implicated in pain and inflammatory responses [4]. Moreover, hEDS skin fibroblasts exhibit a widespread ECM disarray, including that of collagens and fibronectin (FN), and show a

myofibroblast-like phenotype characterized by α-smooth muscle actin (α-SMA) microfilaments organization, cadherin-11 expression, augmented levels of secreted ECM-degrading matrix metalloproteinase 9 (MMP9), enhanced migration, and dysregulated expression of inflammatory mediators [5]. We also demonstrated that in hEDS the fibroblast-to-myofibroblast transition (FMT) is sustained by an αvβ3 integrin-mediated signal transduction pathway involving the integrin linked kinase (ILK) and the transcription factor Snail1/Slug [5,6]. Furthermore, control fibroblasts treated with hEDS culture media acquire this myofibroblast-like phenotype, indicating that patients' cell conditioned medium (CM) contains key factors that control this phenotypic switch [5].

Herein, we performed proteome profiling of dermal myofibroblasts from hEDS patients to uncover potential key molecules involved in the FMT and additional molecular mechanisms related to the disease pathogenesis. Our study provides a proteomic map of dysregulated processes and altered protein networks, thus adding novel insights in the hEDS pathobiology.

## 2. Materials and Methods

### 2.1. Patients, skin biopsies and ethical statement

Written informed consent to the study and for skin biopsy was obtained from 6 hEDS patients and 12 sex- and age-matched healthy donors according to Italian bioethics laws. Skin biopsies were established in our lab by standard protocols, following approval by the local Ethical Committee (Ethical Committee Protocol Number NP3151, Comitato Etico di Brescia, ASST degli Spedali Civili, Brescia). All patients were diagnosed at the specialized outpatient clinic for HCTDs and EDS of the University Hospital Spedali Civili of Brescia according to the 2017 EDS nosology [2]. Four patients (P1, P2, P3, P4) were previously reported [5] and two (P5, P6) were novel. All enrolled patients were adult females with an age range on last evaluation of 38 to 56 years. The corresponding patients' identifier, their classification according to the 2017 EDS nosology, and the detailed description of mucocutaneous, osteoarticular, orthopedic, muscular, gastrointestinal, cardiovascular, neuropsychiatric, uro-gynecological, immunological, and ocular signs are summarized in Supplementary Table 1.

### 2.2. Cell cultures

Cell cultures from skin biopsies derived from 6 adult hEDS females (P1-P6) and 12 unrelated healthy donors (C1-C12) were grown *in vitro* at 37 °C in a 5% $CO_2$ atmosphere in Earle's Modified Eagle Medium supplemented with 2 mM L-glutamine, 10% FBS, and 100 µg/ml penicillin and streptomycin (Life Technologies). Cells were expanded until full confluence and then harvested by 0.25% trypsin/0.02% EDTA treatment. The number of cell passages were between $1^{st}$ – $4^{th}$.

### 2.3. Immunofluorescence microscopy (IF)

To analyze the α-SMA organization and the FN-ECM, control and hEDS cells grown for 72 h on glass coverslides were fixed in cold methanol and immunoreacted for 1 h at room temperature (R.T.) with 2 μg/ml anti-α-SMA monoclonal antibody (mAb) (Sigma Chemicals, clone 1A4) and 1:100 rabbit anti-FN polyclonal Ab (Sigma Aldrich, #F3648), recognizing all human isoforms of the protein, diluted in 1% and 0.3% BSA, respectively. The expression of cadherin-11 was investigated fixing cells in 4% PFA/10 mM sucrose for 10 min, permeabilizing with 0.1% Triton X-100 for 10 min, blocking in 2% BSA/PBS 1x for 1 h at R.T., and immunoreacting for 3 h with 2 μg/ml rabbit anti-CDH11/Cadherin OB Ab (Thermo Fisher Scientific, #71-7600) diluted in 0.1% BSA. The distribution of Snail1/Slug was investigated fixing cells in 3.7% PFA/60 mM sucrose, blocking 30 min at R.T. with 0.1% non-fat milk/0.1% Tween 20/PBS 1x, and immunoreacting O.N. at +4 °C with 1:500 rabbit anti-Snail1/Slug Ab (Abcam, #ab180714) diluted in 0.1% Tween 20/PBS 1x. The organization of non-muscle actin β (β-actin) cytoskeleton and αvβ3 integrin was tested fixing control and hEDS cells in 3% paraformaldehyde/60 mM sucrose and permeabilizing in 0.5% (v/v) Triton X-100. Cells were reacted with 1 μg/ml anti-β-actin (Sigma Chemicals, clone AC-74) and 4 μg/ml mouse anti-αvβ3 integrin (Millipore-Chemicon Int., clone LM609) mAbs. After washing, cells were incubated for 1 h with anti-mouse or anti-rabbit secondary Abs conjugated to Alexa Fluor®594 and 488, respectively. IF signals were acquired by a CCD black-and-white TV camera (SensiCam-PCO Computer Optics GmbH) mounted on a Zeiss fluorescence Axiovert microscope and digitalized by Image Pro Plus software. All experiments were repeated three times.

Before proteome analysis, dermal fibroblasts from the new engaged hEDS patients (P5 and P6) were evaluated by IF for disassembly of the FN-ECM, expression of the alternative FN receptor αvβ3 integrin, organization of the α-SMA cytoskeleton, expression of cadherin-11 and Snail1/Slug, as earlier published [5]. Like the previously reported patients' skin fibroblasts (P1-P4), also the 2 novel hEDS cell strains show these typical myofibroblast-like features. All dermal control fibroblasts included in this work were also analyzed for the absence of these myofibroblast-like markers (Supplementary Figure 1).

## 2.4. Protein extraction

For two-dimensional difference in-gel electrophoresis (2D-DIGE) and label-free liquid Chromatography-Tandem Mass Spectrometry (LC-MS/MS), each cell strain was suspended in lysis buffer (7 M urea, 2 M thiourea, 4% CHAPS, 30 mM Tris, and 1 mM PMSF) and solubilized by sonication on ice. Proteins were selectively precipitated using PlusOne 2D-Clean up Kit (GE Healthcare) to remove non-protein impurities. 2D-DIGE and immunoblot samples were re-suspended in lysis buffer. The pH of the protein extracts was adjusted to pH 8.5 by addition of 1 M NaOH. Label-free LC-MS/MS samples were re-suspended in 50 mM ammonium bicarbonate and 0.1% RapiGest SF surfactant (Waters). Protein concentrations were determined by PlusOne 2D-Quant Kit (GE Healthcare).

## 2.5. Two-dimensional difference in-gel electrophoresis (2D-DIGE)

Whole cell extracts from patients and controls were analyzed by quantitative 2D-DIGE, followed by MS. The 2D-DIGE method was inserted in The Minimum Information About a Proteomics Experiment-Gel Electrophoresis (MIAPE-GE) compliant form [7] in Supplementary Table 2. Protein minimal labeling with cyanine dyes (Cy3 and Cy5), 2D separation, and analyses were performed as previously described [8].

Briefly, 50 μg of each sample extract were mixed with 400 pmol CyDye (GE Healthcare) and incubated, on ice, in the dark for 30 min. The labelling reaction was quenched with 1 ml L-lysine 10 mM on ice for 10 min in the dark. Sample proteins were labelled with Cy5 whereas the internal standard, generated by pooling individual samples (hEDS and controls), was Cy3 labelled. Samples from each subject (40 μg) were combined with an equal amount of internal standard. Each sample was run in triplicate on 24 cm, 3–10 non-linear pH-gradient IPG strips, with a voltage gradient ranging from 200 to 8000 V, for a total of 75 000 Vh, using an IPGphor electrophoresis unit (GE

Healthcare). After focusing, proteins were reduced and alkylated. The second dimension was carried out in 20 × 25 $cm^2$, 12% T, 2.5% C constant concentration polyacrylamide gels at 20 °C, and 15 mA per gel using the Ettan Dalt II system (GE Healthcare). CyDye-labelled gels were visualized and acquired using a Typhoon 9200 Imager (GE Healthcare). Image analysis was performed using the DeCyder version 6.5 software (GE Healthcare).

For each experimental group, spots present in at least 80% of samples were considered. Statistically significant differences of 2D-DIGE data were computed by Student's t-test ($p < 0.05$). False discovery rate (FDR) was applied as a multiple test correction in order to keep the overall error rate as low as possible [9]. Power analysis was conducted on statistically changed spots, and only spots that reached a sensitivity threshold > 0.8 were considered as differentially expressed. Proteins of interest were then identified by MS.

### 2.6. Protein identification by matrix-assisted laser desorption/ionization mass spectrometry (MALDI-TOF MS)

Semipreparative gels, containing 400 µg of total protein extract per strip, were loaded; electrophoretic conditions were the same as for 2D-DIGE, except that gels were stained with a protein fluorescent stain (Krypton, Thermo Fisher Scientific). Image acquisition was performed using the Typhoon 9200 laser scanner. Spots of interest were excised from gel using the Ettan spot picker robotic system (GE Healthcare), destained in 50% methanol/50 mM ammonium bicarbonate, and incubated with 30 µl of 6 ng/µl trypsin (Promega) dissolved in 10 mM ammonium bicarbonate for 16 h at 37 °C. Released peptides were subjected to reverse phase chromatography (Zip-Tip C18 micro, Millipore), eluted with 50% acetonitrile (ACN)/0.1% trifluoroacetic acid. Peptides mixture (1 µl) was diluted in an equal volume of 10 mg/ml alpha-cyano-4-hydroxycinnamic acid matrix dissolved in 70% ACN/30% citric acid 50 mM. Proteins were identified by Peptide Mass Fingerprint (PMF) utilizing a MALDI-TOF mass spectrometer (Ultraflex III TOF/TOF, Bruker

Daltonics), as previously described [10]. In particular, the search was performed by correlation of uninterpreted spectra to entries in UP5640_*H. sapiens* 20201007 database (97057 sequences; 38760527 residues). Protein identification methods are provided in a MIAPE-MS compliant form [7] in Supplementary Table 2.

### 2.7. Label-free liquid chromatography with tandem mass spectrometry (LC-MS/MS)

Protein extracts were reduced for 45 min in 5 mM DTT at 60 °C, carbamidomethylated for 45 min in 15 mM iodoacetamide, and digested with sequence grade trypsin (Promega) for 16 h at 37 °C using a protein:trypsin ratio of 50:1. After acidification with trifluoracetic acid and desalting on C18 tips (Zip-Tip C18 micro, Millipore), peptide samples were vacuum concentrated, reconstituted in HPLC buffer A (0.1% formic acid) and separated on a Dionex UltiMate 3000 HPLC System with an Easy Spray PepMap RSLC C18 column (250 mm, internal diameter of 75 μm) (Thermo Fisher Scientific), adopting a five steps ACN/formic acid gradient (5% ACN in 0.1% formic acid for 5 min, 5–35% ACN in 0.1% formic acid for 139 min, 35–60% ACN in 0.1% formic for 40 min, 60-100% ACN for 1 min, 100% ACN for 10 min, at a flow rate of 0.3 μl/min), and electrosprayed into an Orbitrap Tribrid Fusion (Thermo Fisher Scientific). The LTQ-Orbitrap was operated in positive mode in data-dependent acquisition mode to automatically alternate between a full scan (350–2,000 m/z) in the Orbitrap (at resolution 60000, AGC target 1000000) and subsequent CID MS/MS in the linear ion trap of the 20 most intense peaks from full scan (normalized collision energy of 35%, 10 ms activation). Isolation window: 3 Da, unassigned charge states: rejected, charge state 1: rejected, charge states 2+, 3+, 4+: not rejected; dynamic exclusion enabled (60 s, exclusion list size: 200). Mass spectra were analyzed using MaxQuant software (version 1.6.3.3). The initial maximum allowed mass deviation was set to 6 ppm for monoisotopic precursor ions and 0.5 Da for MS/MS peaks. Enzyme specificity was set to trypsin/P, and a maximum of two missed cleavages were allowed. Carbamidomethylation was set as a fixed modification, while N-terminal acetylation and

methionine oxidation were set as variable modifications. The spectra were searched by the Andromeda search engine against the *H. sapiens* Uniprot sequence database (74823 proteins, release 1 January 2020). Protein identification required at least one unique or razor peptide per protein group. Quantification in MaxQuant was performed using the built in XIC-based label free quantification (LFQ) algorithm using fast LFQ. The required FDR was set to 1% at the peptide, 1% at the protein and 1% at the site-modification level, and the minimum required peptide length was set to 7 amino acids. Statistical analyses were performed using the Perseus software (version 1.4.0.6). Only proteins present and quantified in at least two out of three technical repeats were considered as positively identified in a sample. For each experimental group, the proteins identified in at least 80% of samples were considered. Statistically significant differences were computed by Student's t-test and FDR ($p < 0.05$).

### 2.8. Functional enrichment analyses

To obtain an overview of the biological significance of proteomic changes in hEDS myofibroblasts, we performed Gene Ontology (GO) enrichment analysis by using the online bioinformatic tool DAVID version 6.8 [11]. We included only statistically significant GO terms and clusters of up-and downregulated differentially expressed proteins (DEPs) with an FDR-adjusted p-value < 0.05 and a kappa threshold of 0.7. The freely available software packages PANTHER [12] and STRING v.11 [13] were also queried to identify protein class and potential protein-protein interaction networks, respectively. Criteria for reported functional enrichment required a fold enrichment >1.5, FDR < 0.05, and an adjusted p-value < 0.05.

## 2.9. Protein quantification by immunoblotting

The expression level of a subset of DEPs, i.e., vimentin (VIM), α-parvin (PARVA), cofilin-2 (CFL2), filamin C (FLNC), Rac family small GTPase 1 (RAC1), myosin IC (MYO1C), β-actin, protein disulfide isomerase family A member 3 (PDIA3) RAB1B, member RAS oncogene family (Rab1b), annexin A2 (ANXA2), and S100A4 was evaluated by Western blotting (WB) on pooled cell extracts obtained from $1x10^6$ cells of 6 healthy individuals (C5-C7, C9-C11) and 6 hEDS patients (P1-P6). In addition, the expression of α-SMA was evaluated both in control and hEDS cells, although proteome analysis did not reveal a statically significant difference.

Protein concentration was determined using detergent compatible Bio-Rad Dc Protein Assay (Sigma Aldrich, #1001-491004) and each sample was loaded in triplicate. Specifically, to validate the differential expression of S100A4, ANXA2, VIM, and MYO1C, control and hEDS cells were lysed with RIPA buffer (20 mM Tris HCl pH 7.4, 150 mM NaCl, 0.1% SDS, 1% DOC, 1% Triton X-100, 1 mM EDTA, 0.02 UI/ml aprotinin, 5 μg/ml leupeptin, 1 μg/ml pepstatin, 10 mM NaF, 5 mM $Na_3VO_4$, 1 mM PMSF) and centrifuged at 13,000 rpm at +4 °C for 10 min. 25-50 μg of pooled proteins were separated in reducing conditions by electrophoresis using 5%, 8%, and 12%, SDS-PAGE and after nitrocellulose sheet transfer, membranes were blocked O.N. at 37 °C in 5% non-fat dry milk/TBS-0.1% Tween 20 (TBS-T) and immunoreacted with the following antibodies: 1 μg/ml mouse anti-S100A4 mAb (Novus Biological, clone 1C4), 0.4 μg/ml rabbit anti-MYO1C polyclonal Ab (Abnova, #PAB 30610) diluted in 5% dry milk/TBS-T for 3 h at R.T., 1:1,000 rabbit anti-vimentin mAb (Cell Signalling Tech., clone D21H3) in 5% BSA-TBS-T, and 1:1,000 anti-annexin A2 mAb (Cell Signalling Tech., clone D11G2) in 5% dry milk/TBS-T O.N. at +4 °C. To analyze Rab1B and PDIA3 cells were extracted using RIPA buffer modified with 10 mM Tris HCl pH 7.5 and 0.5% DOC, sonicated three times for 15 sec in ice, 25 μg of pooled proteins were resolved in 8% SDS-PAGE, and immunoreacted with 1:1,000 rabbit anti-Rab1B Ab (Invitrogen, #PA5-77783)

and 1 μg/ml mouse anti-ERp57/PDIA3 mAb (Abcam, clone CL2444) diluted in 5% dry milk/TBS-T for 3 h at R.T.

The cytoskeletal proteins α-SMA, β-actin, PARVA, CFL2, FLNC, and RAC1 were analyzed in control and hEDS pooled cell extracts after lysis with 20 mM Tris HCl pH 7.5, 150 mM NaCl, 0.1% SDS, 1 % Triton X-100, 10 μg/ml leupeptin, 4 μg/ml pepstatin, 10 μg/ml aprotinin, 1 mM $Na_3VO_4$, 10 mM NaF, 10 mM $Na_4P_2O_7$. 80 μg of proteins were resolved in 8% or 5% (for filamin C) SDS-PAGE. Membranes blocked in 5% dry milk/PBS/0.05% Tween20 O.N. at 37 °C were immunoreacted with 2 μg/ml mouse anti-α-SMA (Sigma Chemicals, clone 1A4) and 1 μg/ml anti-β-actin (Sigma Chemicals, clone AC-74) mAbs for 3 h at R.T. Membranes blocked in 5% dry milk/TBS-T O.N. at 37 °C were immunoreacted with 1:1,000 rabbit anti-α-parvin mAb (Cell Signalling Tech., clone D7F9), 0.28 μg/ml rabbit anti-cofilin 2 Ab (GeneTex, #GTX113650), 1.0 μg/ml mouse anti-Rac1 mAb (Abcam, clone 23A8), and 1:1,000 mouse anti-filamin C Ab (Abnova, #H00002318-A01) for 3 h at R.T. The extracellular fraction of S100A4 (e-S100A4) was investigated in pooled control and hEDS CM recovered 48 h from cell seeding, treated O.N. with lysis buffer containing 10 mM Tris HCl pH 6.8, 150 mM NaCl, 1mM EDTA, 0.1% SDS, 1% Triton X-100, 5 μg/ml leupeptin, 1 μg/ml pepstatin, 0.002 UI/ml aprotinin, 5 mM $Na_3VO_4$, 10 mM NaF, 1 mM PMSF, 100 μg of proteins were resolved in a 12% SDS-PAGE under reducing conditions, and the membrane immunoreacted as reported above. After washing in TBS-T, membranes were incubated 2 h at R.T. with HRP-conjugated anti-rabbit or anti-mouse IgGs (Sigma Chemicals, #A8275 and #A5906, respectively) diluted 1:1,000 according to the dilution buffer of the primary Ab, and chemiluminescent signals developed using the ECL method. Band quantification was performed using the Image Pro Plus software (Media Cybernetics) and the intensities were normalized against the total amount of proteins on the membrane stained by Sypro Ruby Protein Blot Stain (Thermo Fisher Scientific, #S-11791). The reported values are the means ± standard error of mean (SEM) of the ratios between the integrated optic density (IOD) of the band and total proteins transferred on the membrane detected in the same lane, loaded in triplicate. Student's t test

was used to compare group means, and a p-value $< 0.05$ was considered statistically significant. Statistical analyses were carried out with the GraphPad Prism software (version 5.0).

## 3. RESULTS

### 3.1. Protein changes in hEDS dermal myofibroblasts

To decipher protein networks and regulatory mechanisms likely involved in the hEDS pathophysiology, we compared the cellular proteome of 6 hEDS dermal myofibroblasts to that of 12 control fibroblasts through a combination of 2D-DIGE and label-free LC-MS/MS analyses. Each approach was performed in triplicate to minimize the variability and increase the reliability of results and statistical analyses. As shown in **Figure 1**, 2D-DIGE revealed a total of 1023 matched spots between all gels and 336 of these were present in at least 80% of gels. After application of statistical criteria (Student's t-test and FDR $p < 0.05$), 32 spots were identified as differentially expressed between hEDS and control cells that corresponded to 11 distinct DEPs (HSP90B1, ANXA6, HSPA2, VCL, PKM, UGDH, PDIA3, VIM, EIF4A1, ACTB, KRT10) as shown by MALDI-ToF MS (Supplementary Table 2). Label-free LC-MS/MS analysis recognized instead a total of 2526 proteins. After filtering those that were present in 2 over 3 technical replicates and in at least 80% of samples per group, 772 proteins were identified. Following the application of Student's t-test and FDR $p < 0.05$, 178 proteins resulted significantly changed in hEDS myofibroblasts compared to control cells, 120 of which showed increased levels and 58 a decreased expression (**Figure 1**, Supplementary Table 3). Amid the 2 approaches, 6 DEPs were shared between the 2 datasets (ANXA6, HSP90B1, UGDH, PDIA3, VIM, ACTB), whereas HSPA2, PKM, VCL, EIF4A1, and KRT10 proteins were identified only by means of 2D-DIGE (**Figure 1**, Supplementary Table 2).

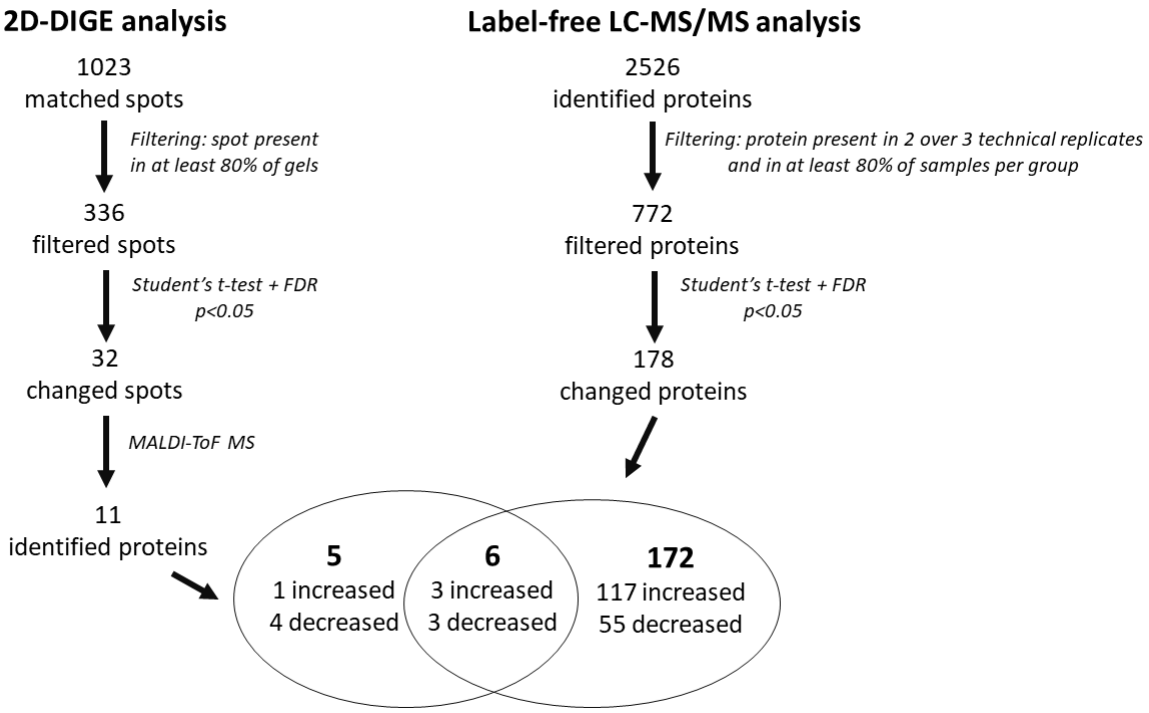


**Figure 1.** Schematic diagram summarizing identification process and findings obtained from 2D-DIGE and label-free LC–MS/MS proteomic analyses of hEDS *vs* control cells. 2D-DIGE led to the identification of 11 varied proteins, whereas label-free LC-MS/MS highlighted 178 changed proteins. Of the 6 proteins in common, 3 were increased and 3 decreased in both datasets.

The final list of 183 DEPs (121 upregulated and 62 downregulated) was then analyzed through bioinformatics software programs, i.e., PANTHER database of protein families, DAVID functional enrichment clustering, and STRING database of protein interactions. As outlined in the PANTHER analysis graph (**Figure 2**), the proteomic survey of hEDS myofibroblasts revealed significant alterations in different protein classes mainly involved in cellular and redox homeostasis (19%), cytoskeleton organization (16%), translation (14%), protein modification (8%), membrane trafficking (8%), calcium binding (7%), transport (7%), as well as with chaperone (4%), adaptor (4%), and nucleic acid binding (3%) functions.

The distribution of identified up- and downregulated DEPs in the different protein families is reported in **Table 1**. Of note, most of the proteins related to metabolism and cell redox balance, translation, calcium binding, and chaperone function showed an increased expression, whereas the majority of proteins with a reduced expression were implicated in the actin cytoskeleton organization and membrane trafficking (**Table 1**).

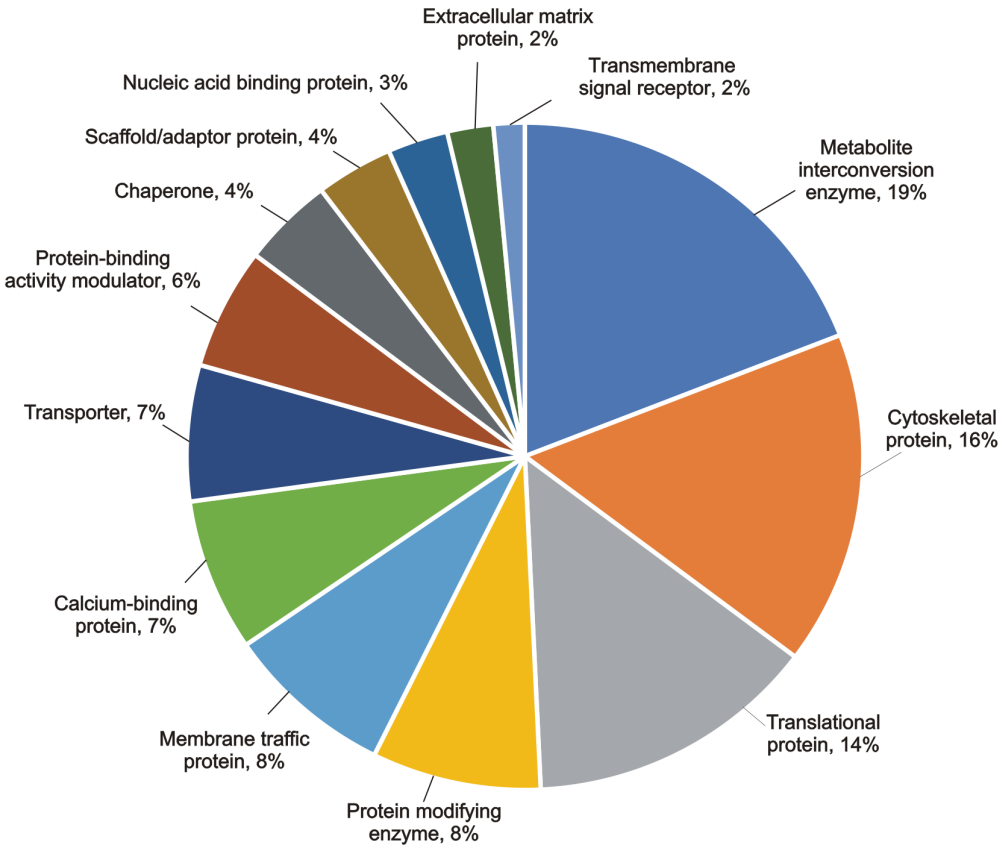


**Figure 2**. Overview of the main altered protein classes in hEDS dermal myofibroblasts according to the PANTHER database.

**Table 1**. **Distribution of up- and downregulated proteins in hEDS compared to control cells based on the PANTHER protein classification**

| PANTHER protein class | DEPs identified in hEDS dermal myofibroblasts |
|---|---|
| Metabolite interconversion enzyme | **CAT**, **GAPDH**, **HINT1**, **SOD1**, **HADHB**, **ECHS1**, **PRDX1**, **GPX1**, **MDH2**, **TKT**, **AK1**, **ACO2**, **PRDX3**, **ACADVL**, **ETFA**, **LDHB**, **FH**, MAT2A, PFKP, TGM2, GLS, QARS, NNMT, SRM |
| Cytoskeletal protein | ACTC1, MYO1C, PDLIM7, WDR1, DNM1L, PLS3, VCL, ACTB, TPM2, TAGLN, PARVA, CNN3, ACTR2, ARPC1A, CSRP1, **MAPRE1, CFL2, VILL, DCTN2, CTTN, COTL1, STOML2** |
| Translational protein | **RPL13**, **EEF1D**, **EIF2S2**, **RPL23**, **RPS5**, **RPS18**, **RPL7A**, **RPS19**, **RPL18**, **RPL12**, **RPS13**, **RPL7**, **RPL10A**, **LRRC47**, **RPL24**, **RPL6**, **EIF3I**, EIF4A1 AARS, WARS |
| Protein modifying enzyme | CUL4B**,** USP5**,** PEPD**,** PREP**,** CAND1**,** SEC11A**, PSMD3, PSMD4, SKP1** |
| Membrane traffic protein | LAMP2, DNM1L, SCARB2, COPE, LAMP1, EHD2, USO1, PICALM, **CLTA**, **CLTB, STX7** |
| Calcium binding protein | **CALM1, CALM2, CALU, S100A4, S100A13, RCN3, ANXA1, ANXA2, ANXA7,** ANXA6 |
| Transporter | **VDAC1**, **VDAC2, ATP5PO**, **STOML2**, **SEC13**, KPNA4, KPNA6, ATP2A2 |
| Protein binding activity modulator | **ARHGDIA, PEBP1, PRKCSH, RAC1, GNAI2,** GNA11**,** GDI2**,** ATL3 |
| Chaperone | **TBCA, CALR, BAG2, HSPE1, HSP90B1, FKBP1B,** HSPA2 |
| Scaffold/adaptor protein | **YWHAQ**, **PLIN3**, **YWHAE**, **RANBP1**, **YWHAZ** |
| Nucleic acid binding protein | **RAD23B, TCEB2, SBDS,** H2AFY |
| Extracellular protein | COL1A1, COL6A1, **LGALS1** |
| Transmembrane signal receptor | **PGRMC1, CD44** |

Proteins with an increased expression are highlighted in bold.

### 3.2. GO enrichment analysis

Functional annotation of global proteome changes was examined using the DAVID database by performing enrichment analysis of biological process, molecular function, and cellular component with a filtering cut-off of at least 5 proteins in each GO term and Fisher exact test (**Figure 3**, Supplementary Table 4).

The 183 DEPs were associated with a total of 45 statistically significant (FDR p-value < 0.05) GO terms for biological process. The most enriched were "cell adhesion" (5.4%), "translational initiation" (5.1%), "rRNA processing" (4.3%), "protein folding" (3.8%), "cell redox homeostasis" (2.3%), and "response to reactive oxygen species" (1.8%) (**Figure 3A**). The most important molecular functions included "protein binding" (37%), "poly(A) RNA binding" (12.4%), "cadherin binding involved in cell-cell adhesion" (7%), followed by "calcium ion binding" (4.6%), "structural constituent of ribosome" (3.8%), and "actin filament binding" (3.3%) (**Figure 3B**). The most enriched GO terms for cellular component were "extracellular exosomes" (31.5%) and "cytoplasm" (24.8%), followed by "focal adhesion" (11.8%), "mitochondrion" (10.3%), "extracellular matrix" (7.2%), "actin cytoskeleton" (3.8%), and "endoplasmic reticulum" (3.6%) (**Figure 3C**, Supplementary Table 4).

To further explore the biological significance of proteome changes, we performed functional annotation clustering of all up- and downregulated proteins by querying the DAVID database (**Tables 2-3**, Supplementary Tables 5 and 6). Functional enrichment analysis of the upregulated proteins revealed 6 major biological GO clusters (**Table 2**).

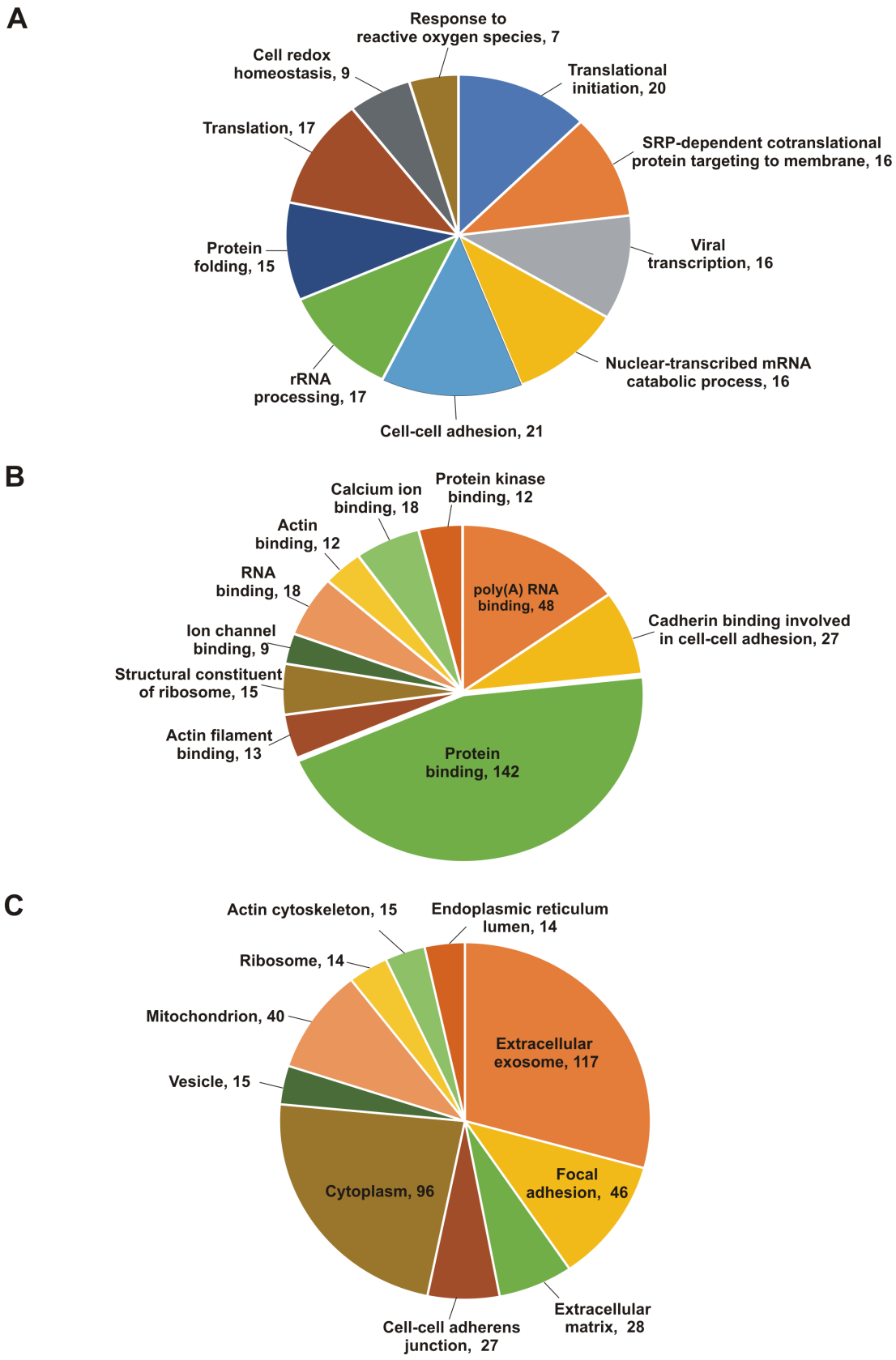


**Figure 3**. GO enrichment analysis of the DEPs in hEDS dermal myofibroblasts according to the DAVID database. The top 10 enriched categories for "biological process" (**A**), "molecular function" (**B**), and "cellular component" (**C**) are shown together with the number of associated proteins in each GO term. The complete list of GO categories is reported in Supplementary Table 4.

The 2 most statistically significant groups contained proteins belonging to the large and small ribosomal subunits with biological functions related to translation and rRNA processing (**Table 2**, Supplementary Table 5). Further upregulated proteins were implicated in energy metabolism including glycolysis, citric acid cycle, and respiratory electron transport [e.g. glyceraldehyde-3-phosphate dehydrogenase (GAPDH), phosphoglycerate mutase 1 (PGAM1), pyruvate kinase M1/2 (PKM), lactate dehydrogenase B (LDHB), ATP synthase membrane subunit g (ATP5MG), ATP synthase peripheral stalk subunit OSCP (ATP5O), ATP synthase F1 subunit gamma (ATP5F1C), fumarate hydratase (FH), malate dehydrogenase 2 (MDH2), aconitase 2 (ACO2), and electron transfer flavoprotein subunit alpha (ETFA)]. Patients' cells also showed a higher expression of proteins involved in endoplasmic reticulum (ER) protein folding [e.g. different members of the protein disulfide isomerase family (PDIA3, PDIA4, PDIA6), calreticulin (CALR), calumenin (CALU), DnaJ heat shock protein family member B11 (DNAJB11), and heat shock protein 90 beta family member 1 (HSP90B1)] and maintenance of redox balance [e.g. superoxide dismutase 1 (SOD1), catalase (CAT), glutathione peroxidase 1 (GPX1), peroxiredoxin 1 (PRDX1), peroxiredoxin 3 (PRDX3), peroxiredoxin 5 (PRDX5), and glutathione S-transferase pi 1 (GSTP1)]. Another significantly enriched GO cluster included calcium related proteins such as three members of the annexin family (ANXA1, ANXA2, ANXA7) and proteins containing a specific calcium-binding domain, known as EF-hand. Among these, there were 2 members of the S100 family (S100A4 and S100A13), calmodulin 1 (CALM1) and calmodulin 2 (CALM2), and some ER-resident proteins such as reticulocalbin 3 (RCN3), peptidyl-prolyl cis–trans isomerase FKBP9, isoform 1 (FKBP9), and CALU. Moreover, GO enrichment analysis also indicated the up-regulated expression of different proteins involved in catabolic process mediated by the proteasome-mediated ubiquitin system (**Table 2**, Supplementary Table 5).

Functional annotation clustering of downregulated proteins highlighted that most of them were involved in actin binding, cytoskeleton organization, and maintenance of focal adhesion and cell-cell junction. Of note, this cluster included more than a few proteins with a calponin homology

domain such as transgelin (TAGLN), calponin 3 (CNN3), actinin alpha 1 (ACTN1), filamin A (FLNA), plastin 3 (PLS3), and parvin alpha (PARVA) (**Table 3**, Supplementary Table 6).

**Table 2**. **DAVID functional annotation clustering of upregulated proteins in hEDS myofibroblasts**

| Cluster | Term description | Count | FDR | Proteins in the cluster |
|---|---|---|---|---|
| 1a | GO:0006413~translational initiation | 19 | 1,17E-15 | RPL23, RPS5, RPL12, RPL10A, EIF2S2, RPL6, RPL7, RPL7A, RPS25, RPS16, RPS19, RPL18A, RPS18, EIF3I, EIF3G, RPL24, RPL13, RPL18, RPS13 |
| 1b | hsa03010:ribosome | 16 | 1,48E-08 | RPL18, RPL13, RPL24, RPS5, RPS25, RPS18, RPS19, RPS16, RPL7, RPL23, RPL18A, RPL6, RPS13, RPL7A, RPL12, RPL10A |
| 2a | GO:0005739~mitochondrion | 31 | 1,30E-08 | YWHAE, FH, ACADVL, ECHS1, GSTP1, RAB1B, HSD17B4, ATP5C1, ETFA, PARK7, ATP5O, ATP5L, PRDX3, LDHB, PRDX5, YWHAQ, C1QBP, PRDX1, CLIC1, GPX1, MDH2, HSPE1, YWHAZ, RAB11B, SOD1, HADHB, PKM, CAT, VDAC2, VDAC1, ACO2 |
| 2b | GO:0005759~mitochondrial matrix | 14 | 2,49E-06 | ACADVL, FH, ECHS1, GPX1, MDH2, ATP5C1, ETFA, PARK7, HSPE1, SOD1, PRDX3, PRDX5, C1QBP, ACO2 |
| 3a | IPR012336:thioredoxin-like fold | 10 | 3,15E-05 | PRDX3, PRDX5, GPX1, GSTP1, PRDX1, SH3BGRL3, PDIA6, CLIC1, PDIA4, TXNDC5 |
| 3b | GO:0045454~cell redox homeostasis | 8 | 7,16E-05 | PRDX3, PRDX5, GPX1, PRDX1, SH3BGRL3, PDIA6, PDIA4, TXNDC5 |
| 4a | GO:0006457~protein folding | 11 | 2,17E-05 | BAG2, PRKCSH, DNAJB11, FKBP9, TBCA, CALR, HSPE1, PDIA6, PDIA4, GNAI2, TXNDC5 |
| 4b | GO:0005788~endoplasmic reticulum lumen | 10 | 5,01E-05 | RCN3, MYDGF, PRKCSH, P4HA2, DNAJB11, CALR, PDIA6, SUMF2, PDIA4, TXNDC5 |
| 4c | hsa04141:protein processing in endoplasmic reticulum | 11 | 0,002 | SEC13, BAG2, PRKCSH, DNAJB11, CALR, PDIA6, RAD23B, CKAP4, PDIA4, SKP1, TXNDC5 |
| 5a | Calcium | 17 | 4,80E-04 | ANXA1, ANXA2, PRKCSH, CLTB, CLTA, SUMF2, RCN3, S100A13, CALU, ANXA7, S100A4, FKBP9, VILL, CALR, CALM1, CALM2 TKT |
| 5b | domain:EF-hand 1 | 8 | 0,009 | RCN3, PRKCSH, S100A13, CALU, S100A4, FKBP9, CALM1, CALM2 |
| 6 | GO:0043161~proteasome-mediated ubiquitin-dependent protein catabolic process | 6 | 0,01 | PSMB6, PSMB5, PSMD4, PSMD3, RAD23B, SKP1 |

**Table 3**. **DAVID functional annotation clustering of downregulated proteins in hEDS myofibroblasts**

| Cluster | Term description | Count | FDR | Proteins in the cluster |
|---|---|---|---|---|
| 1a | GO:0051015~actin binding | 15 | 1,58E-12 | ACTR2, TAGLN, WDR1, TPM2, ACTN1, ARPC1A, DSTN, PARVA, CNN3, VCL, MYO1C, FLNA, PLS3, MYH9, MYH10 |
| 1b | IPR001715:calponin homology domain | 6 | 3,9E-06 | TAGLN, ACTN1, FLNA, PLS3, PARVA, CNN3 |
| 2a | GO:0015629~actin cytoskeleton | 10 | 1,09E-06 | ACTR2, ARPC1A, MYH9, DSTN, FLNA, PARVA, MYH10, VCL, PDLIM7, CNN3 |
| 2b | GO:0051015~actin filament binding | 10 | 8,25E-08 | ACTR2, WDR1, TPM2, ACTN1, ARPC1A, MYH9, DSTN, FLNA, PLS3, MYH10 |
| 2c | GO:0098641~cadherin binding involved in cell-cell adhesion | 8 | 0,002 | USO1, MYH9, FLNA, PARVA, VCL, PFKP, CNN3, PICALM |
| 3a | GO:0005925~focal adhesion | 17 | 8,36E-12 | SCARB2, ACTR2, ACTN1, FHL1, GDI2, PARVA, CNN3, AKAP12, ACTC1, CSRP1, FLNA, MYH9, ITGA5, FERMT2, PDLIM7, VCL, TGM2 |
| 3b | GO:0005911~cell-cell junction | 6 | 0,003 | WDR1, ACTN1, FLNA, ITGA5, VCL, PDLIM7 |
| 3c | hsa04510:focal adhesion | 7 | 0,04 | COL1A1, ACTN1, COL6A2, FLNA, PARVA, ITGA5, VCL |
| 4a | GO:0005524~ATP binding | 16 | 0,003 | ACTR2, EIF4A1, WARS, ATP2A2, HSPA2, EHD2, MYO1C, ACTC1, QARS, MAT2A, LARS, MYH9, MYH10, PFKP, TGM2, AARS |
| 4b | Aminoacyl-tRNA synthetase | 4 | 0,002 | WARS, QARS, LARS, AARS |

### 3.3 Pathways enrichment analysis and protein-protein interaction networks

To identify significant dysregulated pathways and enriched protein domains among the DEPs in hEDS myofibroblasts, we also queried the STRING database (**Table 4**, Supplementary Table 7). This analysis revealed the KEGG pathways "ribosome", "protein processing in endoplasmic reticulum", "carbon metabolism", "metabolic pathways", "biosynthesis of amino acids", "pyruvate metabolism", and "regulation of actin cytoskeleton" as the most perturbed ones. In particular, pathways implicated in metabolic processes, protein translation and processing into the ER lumen, and maintenance of ER proteostasis seem to be enhanced, as suggested by the increased expression of numerous associated proteins. Molecular functions involved in focal adhesion/cell-matrix interactions and fibroblast-specific actin cytoskeleton organization seem to be impaired, given the differential expression of several related proteins, the majority of which were downregulated.

Consistently, also according to the REACTOME database, the most significantly perturbed pathways were related to "metabolism of proteins", "eukaryotic translation", "SRP-dependent co-translational protein targeting to membrane", "vesicle-mediated transport", "cell-extracellular matrix interactions", and "cellular responses to stress" (Supplementary Table S7). Classification of protein families and domains according to the InterPro database further corroborated these findings (**Table 5**, Supplementary Table 7).

The STRING database was also queried to investigate the interaction pattern of DEPs in hEDS myofibroblasts, which confirmed the previous bioinformatic results. Indeed, protein–protein interaction networks of upregulated proteins highlighted potential hubs with biological functions mainly related to ribosome biogenesis and translation, vesicular transport and membrane trafficking, protein quality control including proper protein folding in the ER lumen, cell energy metabolism, and cell redox balance (**Figure 4A**). The most enriched protein clusters of downregulated proteins were actin cytoskeleton organization, tRNA aminoacylation for protein translation, lysosomal transport, ER-Golgi trafficking, and ECM organization (**Figure 4B**).

**Table 4**. **Most significantly perturbed pathways in hEDS myofibroblasts according to the STRING database**

| KEGG ID | Pathway description | Count | FDR | Proteins in the pathway |
|---|---|---|---|---|
| hsa03010 | Ribosome | 16 | 7,16E-11 | **RPL18**, **RPL13**, **RPL24**, **RPS5**, **RPS25**, **RPS18**, **RPS19**, **RPS16**, **RPL7**, **RPL23**, **RPL18A**, **RPL6**, **RPS13**, **RPL7A**, **RPL12**, **RPL10A** |
| hsa04141 | Protein processing in endoplasmic reticulum | 14 | 7,77E-08 | **BAG2**, **CALR**, **CKAP4**, **DNAJB11**, **HSP90B1**, **PDIA3**, **PDIA4**, **PDIA6**, **PRKCSH**, **RAD23B**, **SEC13**, **SKP1**, **TXNDC5,** CRYAB |
| hsa01200 | Carbon metabolism | 10 | 1,58E-05 | **ACO2**, **CAT**, **PKM, ECHS1**, **FH**, **GAPDH**, **MDH2**, PFKP, **PGAM1**, **TKT** |
| hsa01230 | Biosynthesis of amino acids | 7 | 0,00039 | **ACO2, GAPDH,** MAT2A, **PKM, PGAM1,** PFKP, **TKT** |
| hsa05016 | Huntington's disease | 10 | 0,00071 | **ATP5C1**, **ATP5O**, **CLTA**, **CLTB**, **DCTN2**, **GPX1**, **SOD1**, TGM2, **VDAC1**, **VDAC2** |
| hsa01100 | Metabolic pathways | 27 | 0,0012 | **ACADVL**, **ACO2**, **ADK**, **AK1**, **ATP5C1**, **ATP5L**, **ATP5O**, **CBR1**, **ECHS1**, **FH, GAPDH**, GLS, **HADHB**, **HSD17B4**, **LDHB**, MAT2A, **MDH2**, **NAGK**, **NME1**, NNMT, **P4HA2**, PFKP, **PGAM1**, QARS, SRM, **TKT**, UGDH |
| hsa04510 | Focal adhesion | 9 | 0,0029 | VCL, COL1A1, ITGA5, COL6A2, **FLNC**, PARVA, **RAC1**, FLNA, ACTN1 |
| hsa04810 | Regulation of actin cytoskeleton | 9 | 0,0035 | VCL, MYH9, ARPC1A, ITGA5, **CFL2**, **RAC1**, MYH10, ACTN1, **CFL1** |
| hsa00620 | Pyruvate metabolism | 4 | 0,0096 | **PKM**, **MDH2**, **FH**, **LDHB** |

Proteins with an increased expression are highlighted in bold.

**Table 5**. **InterPro classification of the protein families and domains among the DEPs identified in hEDS myofibroblasts**

| InterPro ID | Description | FDR | UniProt KB ID | Proteins name |
|---|---|---|---|---|
| IPR036249 | Thioredoxin-like superfamily | 0,00021 | Q06830, P30044, Q9H299, P13667, P30048, P30101, O00299, Q8NBS9, P09211, Q15084, P07203 | **CLIC1, GPX1, GSTP1, PDIA3, PDIA4, PDIA6, PRDX1, PRDX3, PRDX5, SH3BGRL3, TXNDC5** |
| IPR005788 | Disulphide isomerase | 0,0025 | P13667, P30101, Q8NBS9, Q15084 | **PDIA3, PDIA4, PDIA6, TXNDC5** |
| IPR001715 | Calponin homology domain | 0,00042 | Q14315, Q9NVD7, P13797, P21333, Q15417, Q15691, P12814, Q01995 | ACTN1, CNN3, FLNA, **FLNC**, **MAPRE1**, PARVA, PLS3, TAGLN |
| IPR037104 | Annexin superfamily | 0,0113 | P07355, P08133, P20073, P04083 | **ANXA1, ANXA2,** ANXA6**, ANXA7** |

Proteins with an increased expression are highlighted in bold.

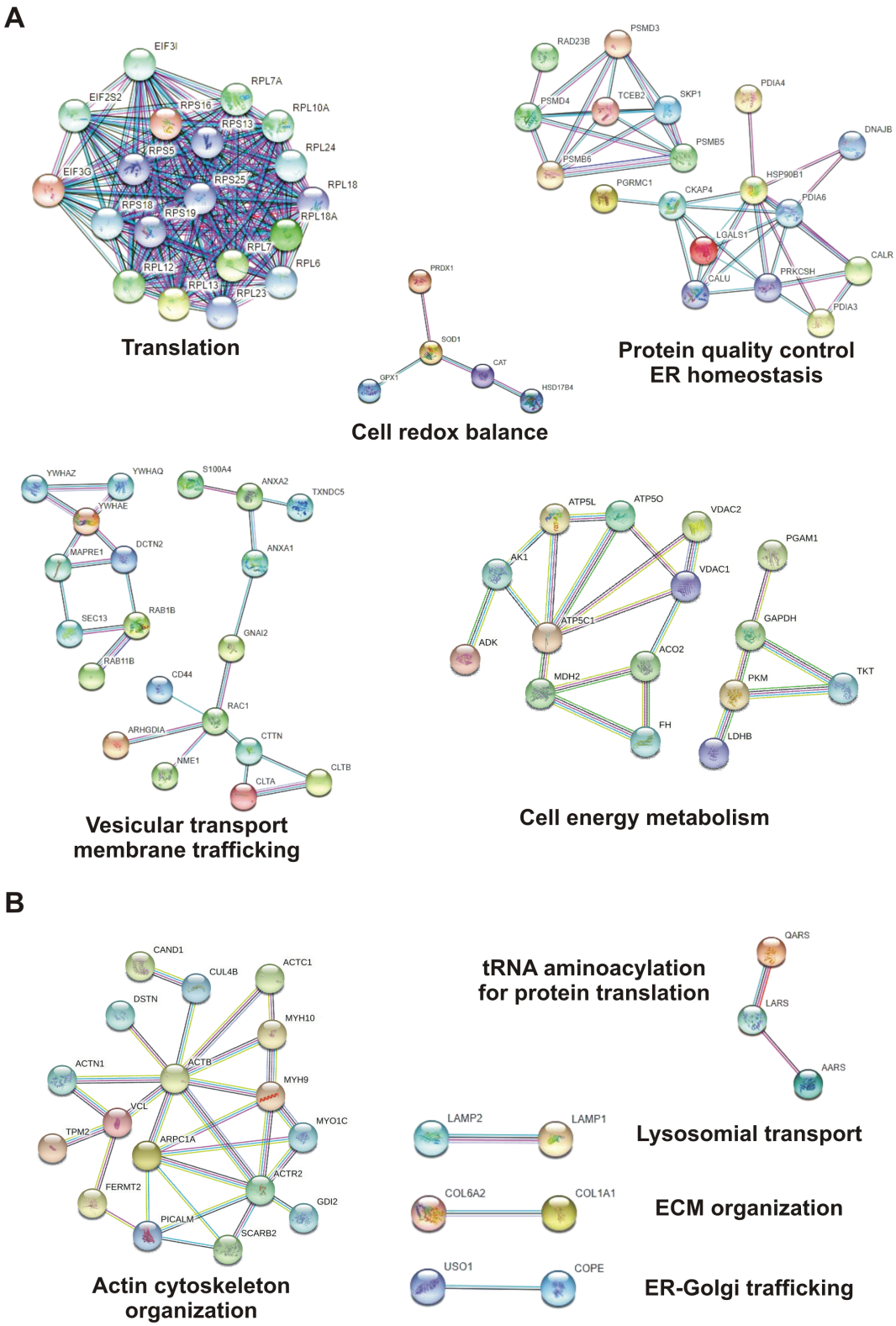


**Figure 4**. Protein-protein interaction networks of up- (**A**) and downregulated (**B**) proteins identified in hEDS myofibroblasts based on the STRING database. Each node represents a protein, and each edge represents an interaction including either physical or functional associations. Only interactions with the highest confidence score (0.9) are shown.

### 3.4. Biochemical analyses by WB and IF

To corroborate the proteomic changes identified in hEDS myofibroblasts, the expression levels of a subset of DEPs related to different cellular pathways, i.e., cytoskeleton organization, intracellular trafficking/vesicular transport, and cell redox homeostasis, were investigated by WB and IF.

Concerning the cytoskeletal organization, WB confirmed the increased protein levels in hEDS *vs* control cells of VIM, CFL2, FLNC, and RAC1, as well as the reduced expression of PARVA, MYO1C, and β-actin (**Figures 5A**,**B**). Although α-SMA was not identified as differentially expressed by proteome analysis, WB demonstrated an increased expression of this myofibroblast specific marker in hEDS compared to control cells (**Figures 5A,B**).

To further verify the rearrangement of the cytoskeleton architecture in hEDS myofibroblasts, the organization of α-SMA and β-actin was evaluated also by IF. As previously reported [5] and shown in **Figure 5C** and Supplementary Figure 1, all hEDS cells included in this study organized α-SMA in cytoskeletal microfilaments, whereas in control cells only intracellular non-fibrillar protein was detectable. In line with the decreased expression of β-actin shown by proteome analysis and WB, IF analysis displayed fragmented fibres of this non muscular actin isoform in hEDS cells compared to controls, which, on the contrary, organized the protein in abundant microfilaments (**Figure 5C**).

WB also confirmed the higher expression in hEDS myofibroblasts of the ER-resident enzyme PDIA3 implicated in protein folding as well as of Rab1b, ANXA2, and S100A4 involved in intracellular trafficking and vesicular transport (**Figures 5A,B**). Since it is known that the S100A4 protein can be secreted trough microvesicles [14], we investigated its presence in the CM (extracellular S100A4, e-S100A4) of control and patient cells. WB analysis revealed significant secreted levels of the e-S100A4 protein only in the CM of hEDS myofibroblasts (**Figure 5A**).

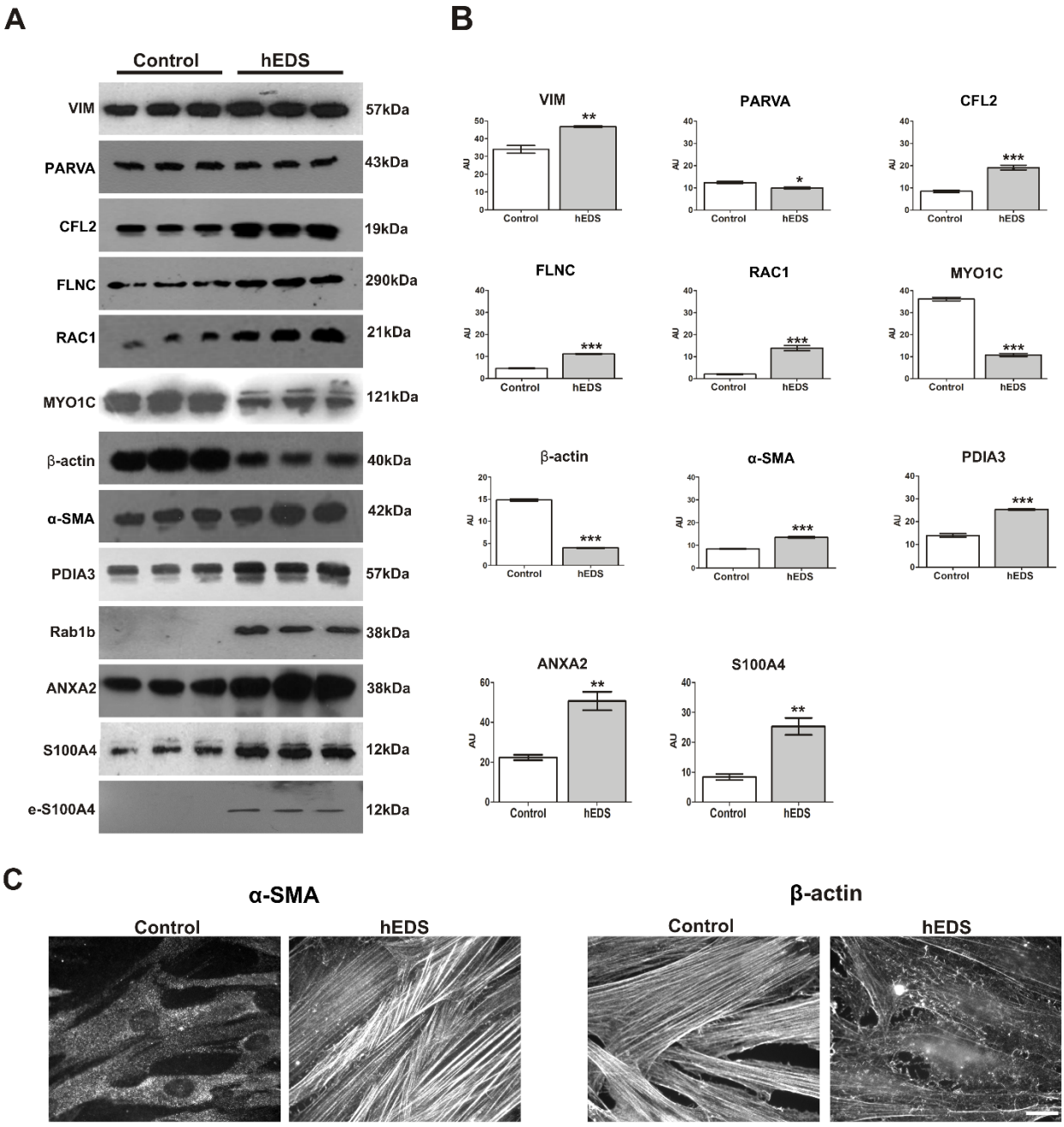


**Figure 5**. Representative WB images (**A**) and respective quantitative analyses (**B**) of protein amounts in pooled whole cell extracts from control fibroblasts (n=6, white bars) and hEDS myofibroblasts (n=6, gray bars) of VIM, PARVA, CFL2, FLNC, RAC1, MYO1C, β-actin, α-SMA, PDIA3, Rab1b, ANXA2, and S100A4. This latter was also analyzed in pooled CM of control and patient cells, starting from 100 µg of proteins recovered after a specific lysis treatment and immunoreacted with the mouse S100A4 mAb, detecting a 12 kDa band (e-S100A4) only in the CM of hEDS myofibroblasts. Protein bands were quantified by image analysis as described in Materials and Methods section. The IOD values were normalized against the total amount of loaded proteins stained with Sypro Ruby Protein Blot Stain. Representative IF analyses (**C**) of α-SMA and β-actin cytoskeleton organization in control and hEDS cells. Scale bar: 9.5 µm. All graphical results are expressed as mean ± SEM of technical triplicates. Statistical analysis was performed with the Student's t-test. * $p < 0.05$, ** $p < 0.01$, *** $p < 0.001$.

## 4. Discussion

Myofibroblasts are highly specialized and differentiated cells that regulate connective tissues remodeling and exhibit cytoskeletal characteristics of contractile smooth muscle cells [15]. They are dynamically involved in response to tissue injury and pathologically contribute to cancer and several fibrotic and inflammatory conditions, as this cell type represents an important source of ECM-remodeling enzymes (e.g. MMPs and their inhibitors) and of inflammatory mediators, cytokines, chemokines, and growth factors [16,17]. Apart from the pathway of the transforming growth factor-β1 (TGF-β1), the most potent and established stimulator of the FMT [16,18], growing evidences on cytoskeleton-dependent signalling and associated mechano-transduction involving integrins and actin remodeling are emerging [19–21]. Indeed, during FMT, the actin cytoskeleton regulates not only mechanical functions (e.g. focal adhesion formation, contraction, ECM remodeling), but it is also involved in transduction of different signals/stimuli (e.g. ECM components, soluble growth factors, and physical force inputs) into biochemical signalling and transcriptional and translational regulation [21,22]. Along with classical cytoskeletal characteristics of myofibroblasts, increasing evidences point to the involvement of mitochondrial alterations and metabolic remodeling in the myofibroblast differentiation. Changes in mitochondrial morphology and activity, including reactive oxidative species (ROS) production, are reported to occur early in myofibroblast formation [23]. Modifications of cellular metabolism, including ATP generation and synthesis of building blocks (e.g. nucleotides, phospholipids, and amino acids), are needed to sustain the biomass required for cellular growth and differentiation, as well as the energetic demand of the acquired contractile phenotype. Indeed, compared with the quiescent state, myofibroblasts increase aerobic glycolysis and lactate production that, in turn, modulate mitochondrial oxidative phosphorylation [24]. Furthermore, recent studies identified variations in mitochondrial and cytosolic calcium dynamics as key mediators linking metabolism to epigenetic modifications required for the FMT [23,24].

In the present study, we performed a comprehensive proteome profiling of 6 hEDS dermal fibroblasts all showing myofibroblast-like features including organization of α-SMA microfilaments, expression of cadherin-11 and αvβ3 integrin, and nuclear localization of the Snail1/Slug transcription factor. Proteomics identified 183 DEPs predicted to perturb numerous biological processes/pathways, among which cytoskeleton remodeling, cell energy metabolism, proteostasis, redox homeostasis, and vesicle trafficking were the most significant.

Consistent with actin cytoskeleton changes essential for the differentiation of fibroblasts to myofibroblasts, hEDS cells showed the differential expression of more than a few cytoskeletal proteins and their interactors. Among these, we found reduced levels of the cytoplasmic β-actin isoform, which, contrary to control cells, was not organized in stress fibers. The decreased expression of regulatory proteins associated with the actin polymerization, i.e., a member of the actin-related protein 2/3 complex (ARPC1A), the actin cross-linker ACTN1, and actin depolymerizing factor destrin (DSTN), likely influences the atypical organization of the actin's network in α-SMA-positive hEDS cells. Furthermore, VIM, one of the most abundant intermediate filaments protein in mesenchymal cells [20], showed higher levels compared to control fibroblasts along with CFL1 and CFL2, which both support actin turnover [25]. FLNA and FLNC were differentially expressed as well; particularly, the ubiquitously expressed FLNA showed a diminished expression, whereas FLNC, the most prevalent isoform in striated muscles, was upregulated. Both proteins crosslink actin filaments and bind to Rho GTPases family members such as RAC1 [26,27], which was also upregulated in hEDS myofibroblasts. This small GTPase, the activation of which is regulated by GDP/GTP-bound conformation changes and through several post-translational modifications [28,29], participates in cell migration, differentiation, and cytoskeletal and cell adhesion dynamics [30,31]. RAC1 activity is controlled by multiple extracellular signals including growth factors, cytokines, integrins (including αvβ3), and mechanical stresses. Concerning signalling through integrins, it is well defined that their downstream effectors (such as ILK) are capable to influence both actin cytoskeleton remodeling

and Rho GTPases activity [32,33]. ILK connects integrins to the cytoskeleton via the so-called IPP complex, comprising ILK itself, PINCH1/2, and the α/β/γ-parvins adaptor proteins [34]. As ILK can only bind one PINCH and one parvin isoform at the same time, this kinase is capable of being part of distinct IPP complexes that may trigger different signalling outputs [35]. In contrast to β-parvin, PARVA appears to be a negative regulator of RAC1 signalling [36,37] and it has been suggested that reduced PARVA amounts in the IPP complex causes RAC1 activation [38]. Since in patients' cells PARVA showed lower levels and RAC1 a higher expression, an enhanced RAC1 activity triggered by the αvβ3/ILK-dependent signalling, which finally leads to the Snail1-mediated FMT [5], can be envisaged. After activation, RAC1 orchestrates many downstream signalling cascades through different effectors or targets including kinases (e.g. ROCKs, PAKs) and actin-nucleating proteins (e.g., Arp2/3 complex and formins). In transformed keratinocytes, it has been proofed that RAC1 mediates TGFβ1-induced epithelial-to-mesenchymal transition (EMT), through the p21-activating kinase (PAK1) by regulating expression of Snail1, as well as MMP9 production/secretion [39]. In chondrocytes from patients with osteoarthritis, RAC1 signalling has been shown to be involved in the cartilage ECM destruction by stimulating MMPs production [40]. In a mouse model of retinitis pigmentosa, it has been suggested that the activation of an αvβ3 integrin/RAC1-dependent pathway by inflammatory molecules (e.g. urokinase-type plasminogen activator) induces the transcription of different genes including inflammatory factors, thus exacerbating chronic inflammation [41]. Based on these studies and our previous and present data, the hypothesis that in the phenotypic switch of hEDS fibroblasts a peculiar cytoskeleton remodeling/signalling, which likely involves αvβ3-ILK complexes in focal adhesion sites, RAC1 and its downstream effectors, is very intriguing. Additional basic research is needed to proof this aspect, which could provide significant insights into the relevance of this signalling pathway in the hEDS pathophysiology.

In line with mitochondrial and metabolic changes contributing to the myofibroblast differentiation and function [23], proteomics recognized a conspicuous group of related DEPs. In particular

dysregulated levels of various mitochondrial proteins, including some subunits of the mitochondrial ATP synthase (ATP5O, ATP5C1, ATP5L) and enzymes involved in oxidative metabolism and fatty acid beta-oxidation (ACO2, MDH2, FH, ACADVL, ECHS1, HADHB, ETFA), and synthesis/turnover of building blocks (TKT, ADK, AK1, NME1, NAGK) were identified. Besides, hEDS myofibroblasts showed higher expression of the glycolytic enzymes GAPDH, PGAM1, and PKM together with the LDHB that is involved in lactate production, thus suggesting that an increased aerobic glycolysis (a.k.a. glycolytic switch) accompanied by decreased glucose oxidation might be involved in the phenotypic differentiation of hEDS fibroblasts. Indeed, several studies have suggested that the reduced glucose oxidation, in face of enhanced glycolytic rates, is a key metabolic driver of myofibroblast differentiation [23,42–46]. For example, it has been shown that the inhibition of aerobic glycolysis prevents the expression of α-SMA, suppresses renal interstitial myofibroblast differentiation [43], and induces the phenotypic reversal of hepatic myofibroblasts into a less mature form [47]. Likewise, the inhibition of LDH prevents the expression of α-SMA [42,45], whereas its overexpression induces myofibroblast differentiation [44]. Notably, in one of these studies it has been demonstrated that the addition of exogenous lactate was sufficient to increase the expression of phenotypic myofibroblast markers in a dose-dependent manner [43]. The mechanisms by which lactate promotes myofibroblast differentiation are not fully explored and range from pH-dependent activation of latent TGF-β in the ECM to epigenetic modifications (e.g. through histone lactylation) regulating gene expression [23,44,48]. These experimental evidences highlighting that changes in metabolism not only associate with the myofibroblast phenotype but are in fact necessary for the myofibroblast differentiation, prompt to further research aimed to unveil the functional significance of metabolic alterations in hEDS.

It is well established that the functional interplay between mitochondria and other cellular organelles, particularly ER, Golgi apparatus, peroxisomes, and lysosomes along with metabolic alterations may perturb several cellular functions [49]. Specifically, mitochondria and ER actively communicate, and their contact sites are key hubs for aerobic metabolism, lipid trafficking, calcium

signalling, ER stress, autophagy, and apoptosis [49]. In this regard, proteome data indicated an increased expression of VDAC1 and VDAC2, which are core components of specialized tethering complexes that function as chaperones to regulate calcium flux from ER to mitochondria, thereby contributing to the intracellular redox balance [49,50]. Besides, the variation of the ER redox state can result in increased mitochondria coupling to ER, which influences ATP production, oxygen consumption, and mitochondrial calcium exchange [51]. In hEDS myofibroblasts, intracellular calcium signaling and ER homeostasis seem to be altered, as suggested not only by the differential expression of VDAC1 and VDAC2 but also by the upregulation of RCN3, CALU, and CALR, which are proteins involved in the calcium storage within the ER lumen and also act as molecular chaperones to promote protein folding [52,53]. These proteins together with other increased chaperones (FKBP9, HSP90B1, BAG2) and members of the PDI family (PDIA3, PDIA4, PDIA6) [54,55] could be associated with robust protein synthesis of activated fibroblasts and/or in recognition of misfolded proteins and response to cellular stress. Likewise, the increased levels of numerous proteins belonging to the core of translation machinery (e.g. ribosomal proteins and translational regulators) and of different proteins involved in ER-associated degradation and ubiquitin–proteasome system (PSMB5, PSMB6, PSMD3, PSMD4, SKP1, RAD23B), further point out a dysregulation of the protein quality control in hEDS cells. Besides, an imbalance of the redox state can also be supposed, considering the upregulation of various antioxidant enzymes (CAT, SOD, GPX1, GSTP1, CBR1, PRDX1, PRDX3, PRDX5), which act as ROS scavengers in different compartments [56]. Together, it is reasonable to assume that in hEDS myofibroblasts several pathways are triggered in response to an unknown molecular defect that affects energy metabolism, proteostasis, calcium homeostasis, and redox balance.

Other deregulated calcium-related proteins were CALM1 and CALM2, which function as intracellular sensors of calcium signalling by mediating the activation of calcium/calmodulin-dependent protein kinases that, in turn, regulate many processes such as cytoskeleton remodeling, cell metabolism, differentiation, and proliferation [57]. Diverse members of the annexin family

(ANXA1, ANXA2, ANXA6, ANXA7), which are involved in signalling, proliferation, and inflammation [58–61], were also differentially expressed. Annexins mediate exocytic and endocytic events, membrane-cytoskeleton linking, and participate in the biogenesis of exosomes, thereby facilitating the loading of a variety of active molecules in the extracellular space [59,62]. Besides annexins, members of the Rab small GTPases family are also involved in the control of intracellular vesicular trafficking [59,63]. In this regard, the ER-Golgi trafficking seems to be altered in hEDS myofibroblasts, as suggested by the differentially expression of some related proteins including the Rab1b, a small GTPase involved in vesicle transport between ER and Golgi [64], the vesicle transport factor USO1 (a.k.a. p115) [65], and members of Golgi-associated myosins (non-muscle myosin IIA, a.k.a. MYH9, and MYO1C), which serve to stabilize branched actin to facilitate the arrival of cargos at the Golgi complex [66].

It is known that annexins form heterotetramers with S100 proteins, which are another group of calcium-binding proteins involved in a wide range of processes, such as proliferation, migration, and differentiation [67]. The establishment of S100-annexins complexes are functionally relevant, since they regulate the organization of membranes and vesicles, thereby participating in the correct disposition of membrane-associated proteins [68]. hEDS myofibroblasts showed high levels of two members of this family, i.e., S100A13 and S100A4, with the latter as the most upregulated protein in patient cells. S100A4 is implicated in disease states of different pro-inflammatory conditions and it is considered a hallmark of the EMT [69–72]. Several proteins have been identified as intracellular S100A4 targets, including liprin β1, methionine aminopeptidase, the p53 tumor suppressor protein, and proteins involved in cytoskeletal rearrangement and cell motility [14,69,72–74]. The latter proteins include filamentous actin (F-actin), tropomyosin (TPM2), MYH9, and MYH10, which were all differentially expressed in hEDS myofibroblasts. S100A4 can also be actively released in the extracellular space by various cell types including fibroblasts [69,70,73]. Of note, S100A4 is not secreted by the classical ER-Golgi route and some evidences showed that cytokine-dependent pathways stimulate the S100A4 secretion through microvesicles shedding from

the plasma membrane [70,75]. S100A4 is classified within the group of molecules called damage-associated molecular patterns (DAMPs), which have critical functions in the activation of innate immunity and secretion of inflammatory mediators [73,76]. Indeed, extracellular S100A4 is a multireceptor ligand that acts as DAMP and regulates several signalling by interacting with more than a few pro-inflammatory surface receptors (e.g. RAGE, ANXA2, TLR4) [72,73]. S100A4 contributes to the pathological ECM remodeling by modulating the production of different structural components as well as matrix degrading proteases [74,77]. Indeed, accumulating evidence revealed a pivotal role of extracellular S100A4 in the establishment of an inflammatory milieu and invasive cellular phenotype by stimulating the production of various MMPs in different cancer and stroma cells [78–82]. Our finding that in hEDS myofibroblasts S100A4 is likely secreted through extracellular vesicles, since it was detectable only in the CM of patient cells after a specific lysis treatment, suggests a potential extracellular role of this protein in the disease pathogenesis. Based on the present findings and in line with our previous data showing that control fibroblasts acquire the hEDS-specific myofibroblast-like phenotype when treated with patient cells' CM [5], it is reasonable to speculate that S100A4 is one of the key disease factors involved in the FMT. S100A4 likely acts either intracellularly and/or as extracellular DAMP by inducing a pro-inflammatory microenvironment characterized by excessive ECM degradation through the stimulation of an enhanced MMPs-mediated proteolytic activity [5]. However, the molecular action by which S100A4 elicits its pathophysiological effect as well as the causal relationship with the hEDS pathogenesis remains to be further investigated. As future expectation, intracellular S100A4 inhibitor compounds (such as niclosamide, calcimycin, LY294002), and/or neutralizing antibodies that specifically target extracellular functions [70,83], and/or MMPs inhibitors such as tetracycline derivatives [84,85], might be promising anti-inflammatory strategies in hEDS that merit further research efforts.

## 5. Conclusions

In summary, this work sheds light into several dysregulated mechanisms and altered protein networks likely involved in the hEDS pathogenesis. Considering the potential role of actin-dependent signalling in integrating multiple inputs promoting ECM remodeling and myofibroblast differentiation and the possible implication of mitochondrial and metabolic changes in controlling cellular differentiation, these may represent attractive pharmacologic targets for hEDS, once investigated more in detail. Likewise, our data provide interesting hints for additional research to decipher mechanisms of action and functional impact of potential bioactive molecule(s) such as S100A4 that might be used or targeted for future therapies in pre-clinical and clinical settings for this molecularly unsolved EDS type.

**Figure legend**

**Supplementary Figure 1**. Organization of FN, αvβ3 integrin, α-SMA cytoskeleton, cadherin-11, and Snail1/Slug expression in hEDS patients P5 and P6, and control cells. IF of FN-ECM, αvβ3 integrin, α-SMA organization, cadherin-11, and Snail1/Slug distribution in 72 h-grown control and hEDS P5 and P6 cells. The organization of α-SMA and αvβ3 integrin as well as the expression of cadherin-11 and Snail1/Slug in hEDS P5 and P6 cells are consistent with a myofibroblast-like phenotype. Scale bar: FN, α-SMA, and cadherin-11 9.5 μm; Scale bar: αvβ3 integrin and Snail1/Slug 6 μm.

Appendix A. Supplementary data

Supplementary data to this article can be found online at xx

**Supplementary Table 1**. Summary of the main clinical features of hEDS patients

**Supplementary Table 2.** MIAPE-GE and MS compliant forms and changed spots identified in hEDS myofibroblasts by 2D-DIGE analysis

**Supplementary Table 3.** Changed proteins in hEDS myofibroblasts identified by label-free LC-MS/MS analysis

**Supplementary Table 4**. Gene Ontology enrichment analysis of identified DEPs in hEDS myofibroblasts according to the DAVID database

**Supplementary Table 5**. DAVID functional annotation clustering of 121 upregulated DEPs in hEDS myofibroblasts

**Supplementary Table 6**. DAVID functional annotation clustering of 62 downregulated DEPs in hEDS myofibroblasts

**Supplementary Table 7**. Top canonical pathways perturbed in hEDS myofibroblasts according to the STRING database

**Acknowledgments**

The work was supported by The Ehlers-Danlos Society [grant number: 2018.02c.LOI.26]. The authors thank the patients for their kind availability for this study and the Fazzo Cusan family for its generous support.

**Declaration of competing interest**

The authors declare no conflict of interest.

**References**


[1] M. Castori, B. Tinkle, H. Levy, R. Grahame, F. Malfait, A. Hakim, A framework for the classification of joint hypermobility and related conditions, Am. J. Med. Genet. Part C Semin. Med. Genet. 175 (2017) 148-157. https://doi.org/10.1002/ajmg.c.31539.

[2] F. Malfait, C. Francomano, P. Byers, J. Belmont, B. Berglund, J. Black, L. Bloom, J.M. Bowen, A.F. Brady, N.P. Burrows, M. Castori, H. Cohen, M. Colombi, S. Demirdas, J. De Backer, A. De Paepe, S. Fournel-Gigleux, M. Frank, N. Ghali, C. Giunta, R. Grahame, A. Hakim, X. Jeunemaitre, D. Johnson, B. Juul-Kristensen, I. Kapferer-Seebacher, H. Kazkaz, T. Kosho, M.E. Lavallee, H. Levy, R. Mendoza-Londono, M. Pepin, F.M. Pope, E. Reinstein, L. Robert, M. Rohrbach, L. Sanders, G.J. Sobey, T. Van Damme, A. Vandersteen, C. van Mourik, N. Voermans, N. Wheeldon, J. Zschocke, B. Tinkle, The 2017 international classification of the Ehlers–Danlos syndromes, Am. J. Med. Genet. Part C Semin. Med. Genet. 175 (2017) 8-26. https://doi.org/10.1002/ajmg.c.31552.

[3] B. Tinkle, M. Castori, B. Berglund, H. Cohen, R. Grahame, H. Kazkaz, H. Levy, Hypermobile Ehlers–Danlos syndrome (a.k.a. Ehlers–Danlos syndrome Type III and Ehlers–Danlos syndrome hypermobility type): Clinical description and natural history, Am. J. Med. Genet. Part C Semin. Med. Genet. 175 (2017) 48-69. https://doi.org/10.1002/ajmg.c.31538.

[4] N. Chiarelli, G. Carini, N. Zoppi, C. Dordoni, M. Ritelli, M. Venturini, M. Castori, M. Colombi, Transcriptome-wide expression profiling in skin fibroblasts of patients with joint hypermobility syndrome/ehlers-danlos syndrome hypermobility type, PLoS One. 11 (2016) e0161347. https://doi.org/10.1371/journal.pone.0161347.

[5] N. Zoppi, N. Chiarelli, S. Binetti, M. Ritelli, M. Colombi, Dermal fibroblast-to-myofibroblast transition sustained by αvß3 integrin-ILK-Snail1/Slug signaling is a common feature for hypermobile Ehlers-Danlos syndrome and hypermobility spectrum disorders, Biochim. Biophys. Acta - Mol. Basis Dis. 1864 (2018) 1010-1023. https://doi.org/10.1016/j.bbadis.2018.01.005.

[6] N. Zoppi, N. Chiarelli, M. Ritelli, M. Colombi, Multifaced roles of the αvβ3 integrin in ehlers–danlos and arterial tortuosity syndromes' dermal fibroblasts, Int. J. Mol. Sci. 19 (2018) 982. https://doi.org/10.3390/ijms19040982.

[7] C.F. Taylor, N.W. Paton, K.S. Lilley, P.A. Binz, R.K. Julian, A.R. Jones, W. Zhu, R. Apweiler, R. Aebersold, E.W. Deutsch, M.J. Dunn, A.J.R. Heck, A. Leitner, M. Macht, M. Mann, L. Martens, T.A. Neubert, S.D. Patterson, P. Ping, S.L. Seymour, P. Souda, A. Tsugita, J. Vandekerckhove, T.M. Vondriska, J.P. Whitelegge, M.R. Wilkins, I. Xenarios, J.R. Yates, H. Hermjakob, The minimum information about a proteomics experiment (MIAPE), Nat. Biotechnol. 25 (2007) 887–893. https://doi.org/10.1038/nbt1329.

[8] C. Gelfi, D. Capitanio, Dige analysis of human tissues, in: Methods Mol. Biol., Humana Press Inc., 2018: pp. 117–136. https://doi.org/10.1007/978-1-4939-7268-5_11.

[9] Y. Benjamini, Y. Hochberg, On the Adaptive Control of the False Discovery Rate in Multiple Testing With Independent Statistics, J. Educ. Behav. Stat. 25 (2000) 60–83. https://doi.org/10.3102/10769986025001060.

[10] D. Capitanio, M. Moriggi, E. Torretta, P. Barbacini, S. De Palma, A. Viganò, H. Lochmüller, F. Muntoni, A. Ferlini, M. Mora, C. Gelfi, Comparative proteomic analyses of Duchenne muscular dystrophy and Becker muscular dystrophy muscles: changes contributing to preserve muscle function in Becker muscular dystrophy patients, J. Cachexia. Sarcopenia Muscle. 11 (2020) 547–563. https://doi.org/10.1002/jcsm.12527.

[11] D.W. Huang, B.T. Sherman, Q. Tan, J. Kir, D. Liu, D. Bryant, Y. Guo, R. Stephens, M.W. Baseler, H.C. Lane, R.A. Lempicki, DAVID Bioinformatics Resources: Expanded annotation database and novel algorithms to better extract biology from large gene lists, Nucleic Acids Res. 35 (2007) 169-175. https://doi.org/10.1093/nar/gkm415.

[12] H. Mi, A. Muruganujan, D. Ebert, X. Huang, P.D. Thomas, PANTHER version 14: More genomes, a new PANTHER GO-slim and improvements in enrichment analysis tools, Nucleic Acids Res. 47 (2019) 419-426. https://doi.org/10.1093/nar/gky1038.

[13] D. Szklarczyk, A.L. Gable, D. Lyon, A. Junge, S. Wyder, J. Huerta-Cepas, M. Simonovic, N.T. Doncheva, J.H. Morris, P. Bork, L.J. Jensen, C. Von Mering, STRING v11: Protein-protein association networks with increased coverage, supporting functional discovery in genome-wide experimental datasets, Nucleic Acids Res. 47 (2019) 607-613. https://doi.org/10.1093/nar/gky1131.

[14] A.R. Bresnick, D.J. Weber, D.B. Zimmer, S100 proteins in cancer, Nat. Rev. Cancer. 15 (2015) 96–109. https://doi.org/10.1038/nrc3893.

[15] B. Hinz, S.H. Phan, V.J. Thannickal, M. Prunotto, A. Desmoulire, J. Varga, O. De Wever, M. Mareel, G. Gabbiani, Recent developments in myofibroblast biology: Paradigms for connective tissue remodeling, Am. J. Pathol. 180 (2012) 1340–1355. https://doi.org/10.1016/j.ajpath.2012.02.004.

[16] M. Michalik, K. Wójcik-Pszczoła, M. Paw, D. Wnuk, P. Koczurkiewicz, M. Sanak, E. Pękala, Z. Madeja, Fibroblast-to-myofibroblast transition in bronchial asthma, Cell. Mol. Life Sci. 75 (2018) 3943–3961. https://doi.org/10.1007/s00018-018-2899-4.

[17] J.M. Carthy, TGFβ signaling and the control of myofibroblast differentiation: Implications for chronic inflammatory disorders, J. Cell. Physiol. 233 (2018) 98–106. https://doi.org/10.1002/jcp.25879.

[18] A. Vallée, Y. Lecarpentier, TGF-β in fibrosis by acting as a conductor for contractile properties of myofibroblasts, Cell Biosci. 9 (2019) 98. https://doi.org/10.1186/s13578-019-0362-3.

[19] D. Duscher, Z.N. Maan, V.W. Wong, R.C. Rennert, M. Januszyk, M. Rodrigues, M. Hu, A.J. Whitmore, A.J. Whittam, M.T. Longaker, G.C. Gurtner, Mechanotransduction and fibrosis, J. Biomech. 47 (2014) 1997–2005. https://doi.org/10.1016/j.jbiomech.2014.03.031.

[20] N. Sandbo, L. V. Smolyaninova, S.N. Orlov, N.O. Dulin, Control of myofibroblast differentiation and function by cytoskeletal signaling, Biochem. 81 (2016) 1698–1708. https://doi.org/10.1134/S0006297916130071.

[21] N. Sandbo, N. Dulin, Actin cytoskeleton in myofibroblast differentiation: ultrastructure defining form and driving function., Transl. Res. 158 (2011) 181–96. https://doi.org/10.1016/j.trsl.2011.05.004.

[22] A. Desmoulière, C. Chaponnier, G. Gabbiani, Tissue repair, contraction, and the myofibroblast, Wound Repair Regen. 13 (2005) 7–12. https://doi.org/10.1111/j.1067-1927.2005.130102.x.

[23] A.A. Gibb, M.P. Lazaropoulos, J.W. Elrod, Myofibroblasts and Fibrosis: Mitochondrial and Metabolic Control of Cellular Differentiation, Circ. Res. 127 (2020) 427–447. https://doi.org/10.1161/CIRCRESAHA.120.316958.

[24] A.A. Lombardi, A.A. Gibb, E. Arif, D.W. Kolmetzky, D. Tomar, T.S. Luongo, P. Jadiya, E.K. Murray, P.K. Lorkiewicz, G. Hajnóczky, E. Murphy, Z.P. Arany, D.P. Kelly, K.B. Margulies, B.G. Hill, J.W. Elrod, Mitochondrial calcium exchange links metabolism with the epigenome to control cellular differentiation, Nat. Commun. 10 (2019) 4509. https://doi.org/10.1038/s41467-019-12103-x.

[25] K. Ohashi, Roles of cofilin in development and its mechanisms of regulation, Dev. Growth Differ. 57 (2015) 275–290. https://doi.org/10.1111/dgd.12213.

[26] J.M. Bellanger, C. Astier, C. Sardet, Y. Ohta, T.P. Stossel, A. Debant, The Rac1- and RhoG-specific GEF domain of trio targets filamin to remodel cytoskeletal actin, Nat. Cell Biol. 2 (2000) 888–892. https://doi.org/10.1038/35046533.

[27] T.P. Stossel, J. Condeelis, L. Cooley, J.H. Hartwig, A. Noegel, M. Schleicher, S.S. Shapiro, Filamins as integrators of cell mechanics and signalling, Nat. Rev. Mol. Cell Biol. 2 (2001) 138–145. https://doi.org/10.1038/35052082.

[28] R.B. Haga, A.J. Ridley, Rho GTPases: Regulation and roles in cancer cell biology, Small GTPases. 7 (2016) 207–221. https://doi.org/10.1080/21541248.2016.1232583.

[29] Margiotta, Bucci, Coordination between Rac1 and Rab Proteins: Functional Implications in Health and Disease, Cells. 8 (2019) 396. https://doi.org/10.3390/cells8050396.

[30] R.G. Hodge, A.J. Ridley, Regulating Rho GTPases and their regulators, Nat. Rev. Mol. Cell Biol. 17 (2016) 496–510. https://doi.org/10.1038/nrm.2016.67.

[31] H. Marei, A. Malliri, Rac1 in human diseases: The therapeutic potential of targeting Rac1 signaling regulatory mechanisms, Small GTPases. 8 (2017) 139–163. https://doi.org/10.1080/21541248.2016.1211398.

[32] G. Hannigan, A.A. Troussard, S. Dedhar, Integrin-linked kinase: A cancer therapeutic target unique among its ILK, Nat. Rev. Cancer. 5 (2005) 51–63. https://doi.org/10.1038/nrc1524.

[33] S.J. Heasman, A.J. Ridley, Mammalian Rho GTPases: New insights into their functions from in vivo studies, Nat. Rev. Mol. Cell Biol. 9 (2008) 690–701. https://doi.org/10.1038/nrm2476.

[34] N. Rooney, C.H. Streuli, How integrins control mammary epithelial differentiation: A possible role for the ILK-PINCH-Parvin complex, FEBS Lett. 585 (2011) 1663–1672. https://doi.org/10.1016/j.febslet.2011.05.014.

[35] M. Widmaier, E. Rognoni, K. Radovanac, S.B. Azimifar, R. Fässler, Integrin-linked kinase at a glance, J. Cell Sci. 125 (2012) 1839–1843. https://doi.org/10.1242/jcs.093864.

[36] J.L. Sepulveda, C. Wu, The parvins, Cell. Mol. Life Sci. 63 (2006) 25–35. https://doi.org/10.1007/s00018-005-5355-1.

[37] Y. Zhang, K. Chen, Y. Tu, C. Wu, Distinct roles of two structurally closely related focal adhesion proteins, α-parvins and β-parvins, in regulation of cell morphology and survival, J. Biol. Chem. 279 (2004) 41695–41705. https://doi.org/10.1074/jbc.M401563200.

[38] H. Chen, X.N. Huang, W. Yan, K. Chen, L. Guo, L. Tummalapali, S. Dedhar, R. St-Arnaud, C. Wu, J.L. Sepulveda, Role of the integrin-linked kinase/PINCH1/alpha-parvin complex in cardiac myocyte hypertrophy, Lab. Investig. 85 (2005) 1342–1356. https://doi.org/10.1038/labinvest.3700345.

[39] J.F. Santibáñez, J. Kocić, A. Fabra, A. Cano, M. Quintanilla, Rac1 modulates TGF-β1-mediated epithelial cell plasticity and MMP9 production in transformed keratinocytes, FEBS

Lett. 584 (2010) 2305–2310. https://doi.org/10.1016/j.febslet.2010.03.042.

[40] D.L. Long, J.S. Willey, R.F. Loeser, Rac1 is required for matrix metalloproteinase 13 production by chondrocytes in response to fibronectin fragments, Arthritis Rheum. 65 (2013) 1561–1568. https://doi.org/10.1002/art.37922.

[41] M. Cammalleri, M. Dal Monte, F. Locri, V. Pecci, M. De Rosa, V. Pavone, P. Bagnoli, The urokinase-type plasminogen activator system as drug target in retinitis pigmentosa: New pre-clinical evidence in the rd10 mouse model, J. Cell. Mol. Med. 23 (2019) 5176–5192. https://doi.org/10.1111/jcmm.14391.

[42] Y. Chen, S.S. Choi, G.A. Michelotti, I.S. Chan, M. Swiderska-Syn, G.F. Karaca, G. Xie, C.A. Moylan, F. Garibaldi, R. Premont, H.B. Suliman, C.A. Piantadosi, A.M. Diehl, Hedgehog controls hepatic stellate cell fate by regulating metabolism, Gastroenterology. 143 (2012) 1319-1329. https://doi.org/10.1053/j.gastro.2012.07.115.

[43] H. Ding, L. Jiang, J. Xu, F. Bai, Y. Zhou, Q. Yuan, J. Luo, K. Zen, J. Yang, Inhibiting aerobic glycolysis suppresses renal interstitial fibroblast activation and renal fibrosis, Am. J. Physiol. - Ren. Physiol. 313 (2017) F561–F575. https://doi.org/10.1152/ajprenal.00036.2017.

[44] R.M. Kottmann, A.A. Kulkarni, K.A. Smolnycki, E. Lyda, T. Dahanayake, R. Salibi, S. Honnons, C. Jones, N.G. Isern, J.Z. Hu, S.D. Nathan, G. Grant, R.P. Phipps, P.J. Sime, Lactic acid is elevated in idiopathic pulmonary fibrosis and induces myofibroblast differentiation via pH-dependent activation of transforming growth factor-β, Am. J. Respir. Crit. Care Med. 186 (2012) 740–751. https://doi.org/10.1164/rccm.201201-0084OC.

[45] R.M. Kottmann, E. Trawick, J.L. Judge, L.A. Wahl, A.P. Epa, K.M. Owens, T.H. Thatcher, R.P. Phipps, P.J. Sime, Pharmacologic inhibition of lactate production prevents myofibroblast differentiation, Am. J. Physiol. - Lung Cell. Mol. Physiol. 309 (2015) L1305–L1312. https://doi.org/10.1152/ajplung.00058.2015.

[46] N. Xie, Z. Tan, S. Banerjee, H. Cui, J. Ge, R.M. Liu, K. Bernard, V.J. Thannickal, G. Liu, Glycolytic reprogramming in myofibroblast differentiation and lung fibrosis, Am. J. Respir.

Crit. Care Med. 192 (2015) 1462–1474. https://doi.org/10.1164/rccm.201504-0780OC.

[47] S. Karthikeyan, J.J. Potter, J.F. Geschwind, S. Sur, J.P. Hamilton, B. Vogelstein, K.W. Kinzler, E. Mezey, S. Ganapathy-Kanniappan, Deregulation of energy metabolism promotes antifibrotic effects in human hepatic stellate cells and prevents liver fibrosis in a mouse model, Biochem. Biophys. Res. Commun. 469 (2016) 463–469. https://doi.org/10.1016/j.bbrc.2015.10.101.

[48] D. Zhang, Z. Tang, H. Huang, G. Zhou, C. Cui, Y. Weng, W. Liu, S. Kim, S. Lee, M. Perez-Neut, J. Ding, D. Czyz, R. Hu, Z. Ye, M. He, Y.G. Zheng, H.A. Shuman, L. Dai, B. Ren, R.G. Roeder, L. Becker, Y. Zhao, Metabolic regulation of gene expression by histone lactylation, Nature. 574 (2019) 575–580. https://doi.org/10.1038/s41586-019-1678-1.

[49] I. Gordaliza-Alaguero, C. Cantó, A. Zorzano, Metabolic implications of organelle–mitochondria communication, EMBO Rep. 20 (2019) e47928. https://doi.org/10.15252/embr.201947928.

[50] G. Szabadkai, K. Bianchi, P. Várnai, D. De Stefani, M.R. Wieckowski, D. Cavagna, A.I. Nagy, T. Balla, R. Rizzuto, Chaperone-mediated coupling of endoplasmic reticulum and mitochondrial Ca2+ channels, J. Cell Biol. 175 (2006) 901–911. https://doi.org/10.1083/jcb.200608073.

[51] R. Bravo, J.M. Vicencio, V. Parra, R. Troncoso, J.P. Munoz, M. Bui, C. Quiroga, A.E. Rodriguez, H.E. Verdejo, J. Ferreira, M. Iglewski, M. Chiong, T. Simmen, A. Zorzano, J.A. Hill, B.A. Rothermel, G. Szabadkai, S. Lavandero, Increased ER-mitochondrial coupling promotes mitochondrial respiration and bioenergetics during early phases of ER stress, J. Cell Sci. 124 (2011) 2511. https://doi.org/10.1242/jcs.095455.

[52] I. Vandecaetsbeek, P. Vangheluwe, L. Raeymaekers, F. Wuytack, J. Vanoevelen, The Ca2+ Pumps of the Endoplasmic Reticulum and Golgi Apparatus, Cold Spring Harb. Perspect. Biol. 3 (2011) 1–24. https://doi.org/10.1101/cshperspect.a004184.

[53] G. Kozlov, K. Gehring, Calnexin cycle – structural features of the ER chaperone system,

FEBS J. (2020) febs.15330. https://doi.org/10.1111/febs.15330.

[54] L. Ellgaard, E.M. Frickel, Calnexin, calreticulin, and ERp57: Teammates in glycoprotein folding, Cell Biochem. Biophys. 39 (2003) 223–247. https://doi.org/10.1385/CBB:39:3:223.

[55] P. Määttänen, K. Gehring, J.J.M. Bergeron, D.Y. Thomas, Protein quality control in the ER: The recognition of misfolded proteins, Semin. Cell Dev. Biol. 21 (2010) 500–511. https://doi.org/10.1016/j.semcdb.2010.03.006.

[56] E. Veal, T. Jackson, H. Latimer, Role/s of 'antioxidant' enzymes in ageing, in: Subcell. Biochem., Springer New York, 2018: pp. 425–450. https://doi.org/10.1007/978-981-13-2835-0_14.

[57] K.L. Marcelo, A.R. Means, B. York, The Ca2+/Calmodulin/CaMKK2 Axis: Nature's Metabolic CaMshaft, Trends Endocrinol. Metab. 27 (2016) 706–718. https://doi.org/10.1016/j.tem.2016.06.001.

[58] V. Gerke, C.E. Creutz, S.E. Moss, Annexins: Linking Ca2+ signalling to membrane dynamics, Nat. Rev. Mol. Cell Biol. 6 (2005) 449–461. https://doi.org/10.1038/nrm1661.

[59] C. Rentero, P. Blanco-Muñoz, E. Meneses-Salas, T. Grewal, C. Enrich, Annexins—coordinators of cholesterol homeostasis in endocytic pathways, Int. J. Mol. Sci. 19 (2018) 1444. https://doi.org/10.3390/ijms19051444.

[60] C. Enrich, C. Rentero, E. Meneses-Salas, F. Tebar, T. Grewal, Annexins: Ca2+ effectors determining membrane trafficking in the late endocytic compartment, in: Adv. Exp. Med. Biol., Springer New York LLC, 2017: pp. 351–385. https://doi.org/10.1007/978-3-319-55858-5_14.

[61] V. Dallacasagrande, K.A. Hajjar, Annexin A2 in Inflammation and Host Defense, Cells. 9 (2020) 1499. https://doi.org/10.3390/cells9061499.

[62] G. Van Niel, G. D'Angelo, G. Raposo, Shedding light on the cell biology of extracellular vesicles, Nat. Rev. Mol. Cell Biol. 19 (2018) 213–228. https://doi.org/10.1038/nrm.2017.125.

[63] A.H. Hutagalung, P.J. Novick, Role of Rab GTPases in membrane traffic and cell physiology, Physiol. Rev. 91 (2011) 119–149. https://doi.org/10.1152/physrev.00059.2009.

[64] X.Z. Yang, X.X. Li, Y.J. Zhang, L. Rodriguez-Rodriguez, M.Q. Xiang, H.Y. Wang, X.F.S. Zheng, Rab1 in cell signaling, cancer and other diseases, Oncogene. 35 (2016) 5699–5704. https://doi.org/10.1038/onc.2016.81.

[65] E. Giacomello, P. Ronchi, R. Pepperkok, GM130 and p115 play a key role in the organisation of the early secretory pathway during skeletal muscle differentiation, J. Cell Sci. 132 (2019) jcs222083. https://doi.org/10.1242/jcs.222083.

[66] A. Capmany, A. Yoshimura, R. Kerdous, V. Caorsi, A. Lescure, E. Del Nery, E. Coudrier, B. Goud, K. Schauer, MYO1C stabilizes actin and facilitates the arrival of transport carriers at the Golgi complex, J. Cell Sci. 132 (2019) jcs225029. https://doi.org/10.1242/jcs.225029.

[67] E. Leclerc, The importance of Ca2+/Zn2+ signaling S100 proteins and RAGE in translational medicine, Front. Biosci. S3 (2011) 1232. https://doi.org/10.2741/223.

[68] N. Miwa, T. Uebi, S. Kawamura, S100-annexin complexes - biology of conditional association, FEBS J. 275 (2008) 4945–4955. https://doi.org/10.1111/j.1742-4658.2008.06653.x.

[69] M. Schneider, J.L. Hansen, S.P. Sheikh, S100A4: A common mediator of epithelial-mesenchymal transition, fibrosis and regeneration in diseases?, J. Mol. Med. 86 (2008) 507–522. https://doi.org/10.1007/s00109-007-0301-3.

[70] Z. Li, Y. Li, S. Liu, Z. Qin, Extracellular S100A4 as a key player in fibrotic diseases, J. Cell. Mol. Med. 24 (2020) 5973–5983. https://doi.org/10.1111/jcmm.15259.

[71] Q. Ning, F. Li, L. Wang, H. Li, Y. Yao, T. Hu, Z. Sun, S100A4 amplifies TGF-β-induced epithelial–mesenchymal transition in a pleural mesothelial cell line, J. Investig. Med. 66 (2018) 334–339. https://doi.org/10.1136/jim-2017-000542.

[72] F. Fei, J. Qu, C. Li, X. Wang, Y. Li, S. Zhang, Role of metastasis-induced protein S100A4 in human non-tumor pathophysiologies, Cell Biosci. 7 (2017) 64.

https://doi.org/10.1186/s13578-017-0191-1.

[73] N. Ambartsumian, J. Klingelhöfer, M. Grigorian, The multifaceted S100A4 protein in cancer and inflammation, in: Methods Mol. Biol., Humana Press Inc., 2019: pp. 339–365. https://doi.org/10.1007/978-1-4939-9030-6_22.

[74] S.C. Garrett, K.M. Varney, D.J. Weber, A.R. Bresnick, S100A4, a mediator of metastasis, J. Biol. Chem. 281 (2006) 677–680. https://doi.org/10.1074/jbc.R500017200.

[75] B. Forst, M.T. Hansen, J. Klingelhöfer, H.D. Möller, G.H. Nielsen, B. Grum-Schwensen, N. Ambartsumian, E. Lukanidin, M. Grigorian, Metastasis-inducing S100A4 and RANTES cooperate in promoting tumor progression in mice, PLoS One. 5 (2010) e10374. https://doi.org/10.1371/journal.pone.0010374.

[76] J.K. Chan, J. Roth, J.J. Oppenheim, K.J. Tracey, T. Vogl, M. Feldmann, N. Horwood, J. Nanchahal, Alarmins: Awaiting a clinical response, J. Clin. Invest. 122 (2012) 2711–2719. https://doi.org/10.1172/JCI62423.

[77] R. Donato, B. R. Cannon, G. Sorci, F. Riuzzi, K. Hsu, D. J. Weber, C. L. Geczy, Functions of S100 Proteins, Curr. Mol. Med. 13 (2012) 24–57. https://doi.org/10.2174/156652413804486214.

[78] G. Zhang, M. Li, J. Jin, Y. Bai, C. Yang, Knockdown of S100A4 decreases tumorigenesis and metastasis in osteosarcoma cells by repression of matrix metalloproteinase-9, Asian Pacific J. Cancer Prev. 12 (2011) 2075–2080.

[79] M. Saleem, M.H. Kweon, J.J. Johnson, V.M. Adhami, I. Elcheva, N. Khan, B. Bin Hafeez, K.M.R. Bhat, S. Sarfaraz, S. Reagan-Shaw, V.S. Spiegelman, V. Setaluri, H. Mukhtar, S100A4 accelerates tumorigenesis and invasion of human prostate cancer through the transcriptional regulation of matrix metalloproteinase 9, Proc. Natl. Acad. Sci. U. S. A. 103 (2006) 14825–14830. https://doi.org/10.1073/pnas.0606747103.

[80] L. André S Cerezo, M. Remá Ková, M. Tomč Ik, S. Gay, M. Neidhart, E. Lukanidin, K. Pavelka, M. Grigorian, J. Vencovsky´1, V. Vencovsky´1, L.S.ˇ Enolt, The metastasis-

associated protein S100A4 promotes the inflammatory response of mononuclear cells via the TLR4 signalling pathway in rheumatoid arthritis, 53 (2014) 1520-1526. https://doi.org/10.1093/rheumatology/keu031.

[81] C. Chaabane, C.W. Heizmann, M.L. Bochaton-Piallat, Extracellular S100A4 induces smooth muscle cell phenotypic transition mediated by RAGE, Biochim. Biophys. Acta - Mol. Cell Res. 1853 (2015) 2144–2157. https://doi.org/10.1016/j.bbamcr.2014.07.022.

[82] B. Schmidt-Hansen, D. Örnås, M. Grigorian, J. Klingelhöfer, E. Tulchinsky, E. Lukanidin, N. Ambartsumian, Extracellular S100A4(mts1) stimulates invasive growth of mouse endothelial cells and modulates MMP-13 matrix metalloproteinase activity, Oncogene. 23 (2004) 5487–5495. https://doi.org/10.1038/sj.onc.1207720.

[83] B. Grum-Schwensen, J. Klingelhöfer, M. Beck, M.M. Bonefeld, P. Hamerlik, P. Guldberg, M. Grigorian, E. Lukanidin, N. Ambartsumian, S100A4-neutralizing antibody suppresses spontaneous tumor progression, pre-metastatic niche formation and alters T-cell polarization balance, BMC Cancer. 15 (2015) 44. https://doi.org/10.1186/s12885-015-1034-2.

[84] S.S. Parvathy, W. Masocha, Matrix metalloproteinase inhibitor COL-3 prevents the development of paclitaxel-induced hyperalgesia in mice, Med. Princ. Pract. 22 (2012) 35–41. https://doi.org/10.1159/000341710.

[85] M. Valero-Muñoz, R.M. Wilson, R. Bretón-Romero, D. Croteau, D.C. Seldin, F. Sam, Doxycycline decreases amyloidogenic light chain-induced autophagy in isolated primary cardiac myocytes, Int. J. Cardiol. S0167-5273 (2020) 33464-1. https://doi.org/10.1016/j.ijcard.2020.07.016.